FINAL REPORT

Multifractal Characterization of Geologic Noise for Improved UXO Detection and Discrimination

SERDP Project MM-1508

March 2008

Dr. Jonthan E. Nyquist and Dr. Michel Boufadel,
Temple University

DoD EPA DOE SERDP
Strategic Environmental Research and Development Program

Report Documentation Page

Form Approved
OMB No. 0704-0188

1. REPORT DATE	2. REPORT TYPE	3. DATES COVERED
01 MAR 2008	**N/A**	**-**

4. TITLE AND SUBTITLE	5a. CONTRACT NUMBER
Multifractal Characterization of Geologic Noise for Improved UXO Detection and Discrimination	5b. GRANT NUMBER
	5c. PROGRAM ELEMENT NUMBER
6. AUTHOR(S)	5d. PROJECT NUMBER
	5e. TASK NUMBER
	5f. WORK UNIT NUMBER
7. PERFORMING ORGANIZATION NAME(S) AND ADDRESS(ES) **Temple University**	8. PERFORMING ORGANIZATION REPORT NUMBER
9. SPONSORING/MONITORING AGENCY NAME(S) AND ADDRESS(ES)	10. SPONSOR/MONITOR'S ACRONYM(S)
	11. SPONSOR/MONITOR'S REPORT NUMBER(S)

12. DISTRIBUTION/AVAILABILITY STATEMENT
Approved for public release, distribution unlimited

13. SUPPLEMENTARY NOTES
The original document contains color images.

14. ABSTRACT

15. SUBJECT TERMS

16. SECURITY CLASSIFICATION OF:			17. LIMITATION OF ABSTRACT	18. NUMBER OF PAGES	19a. NAME OF RESPONSIBLE PERSON
a. REPORT	b. ABSTRACT	c. THIS PAGE			
unclassified	**unclassified**	**unclassified**	**UU**	**40**	

Standard Form 298 (Rev. 8-98)
Prescribed by ANSI Std Z39-18

Executive Summary

Pushing sensors and algorithms to the limit to minimize the chance of overlooking unexploded ordnance (UXO) increases the chance that noise will be misidentified as signal and money wasted excavating scrap metal or chucks of magnetic rock. Approaches to improve the signal to noise ratio typically follow one of three tracks: (1) development of new sensors that are either more sensitive, or less noisy; (2) fusion of data from multiple sensors so that the chances of confounding all of the det6ectors simultaneously is reduced; or (3) development of computer algorithms to extract the signal(s) from the noise. In the case of wide-area surveys that use methods such as helicopter-borne magnetometry, the battle against noise has focused primarily on instrument noise (e.g., thermal noise), platform noise (e.g., magnetic noise created by the helicopter), or interference created by multiple UXO targets in cluttered settings. What has been largely ignored is the "noise" created by the rock and soil that surrounds the buried ordnance.

The goal of this pilot project was to investigate a new approach to the characterization and simulation of geologic noise using multifractal analysis that captures the scale-dependent variability arising from geologic heterogeneity in different environments. By combining geologic noise simulations with models for the geophysical signatures of UXO, the researchers aim to create synthetic datasets that can be used both to test and improve UXO discrimination algorithms developed by other researchers, and to develop more reliable estimates of the ratio of false positives to false negatives for a particular geologic environment.

In this report we discuss the multifractal methodology and its application to three data sets: Isleta Pueblo, NM; Fort Ord, CA; and the Sierra Army Depot, CA, The S1 site at the Isleta Pueblo, which is underlain by volcanic rock, typifies a UXO site with high magnetic noise. Fort Ord is underlain by sedimentary rock that is largely non-magnetic, but apparently magnetic sediments have washed into topographic drainages, creating moderate levels of geologic noise distributed anisotropically across the site. The Sierra Army Depot rests on a thick sediment-filled graben that is low in magnetic minerals so represents a geologic environment with magnetic noise levels as low as is found anywhere. Thus, the three data sets encompass a wide range of geologic conditions likely to be encountered at UXO sites.

Tests showed the data to be multifractal, and our simulation results demonstrate that the multifractal methodology provides a versatile tool for researchers to experiment with new detection and discrimination algorithms, and could potentially be used for QA assessment at UXO remediation sites. Future work might focus on improved methods for characterizing and modeling anisotropy, on incorporating remnant magnetization, and on joint multifractal modeling of other geophysical properties such as electrical conductivity and dielectric permeability.

Table of Contents

Introduction

The Problem of UXO Detection and Discrimination

Scientific measurement, whether looking at spectra from distant galaxies or searching for irregularities in the EKG of a heart patient, invariably revolves around a struggle to extract signal from noise, giving rise to the twin detection problems of false positives and false negatives. These two errors are complementary: raise instrument detection thresholds to avoid false positives, you increase the chance of missing the signal, a false negative. Conversely, lower the detection threshold to avoid false negatives, you increase the risk of misidentifying noise as signal, a false positive.

The latter problem of false positives is particularly acute when seeking to map unexploded ordnance (UXO). To minimize the danger of leaving ordnance behind virtually every anomaly detected that could conceivably be a munition item must be excavated. Consequently, millions of dollars are spent each year digging up scrap metal, and in many cases, naturally magnetic soil and rock. Butler (2003) describes a typical scenario of a $30 million remediation program where 76% of the budget is expended on non-UXO removal (Figure 1). In extreme cases, such as Kaho'olawe, Hawaii, of 49,521 anomalies excavated, only 3% were UXO (Putnam, 2001).

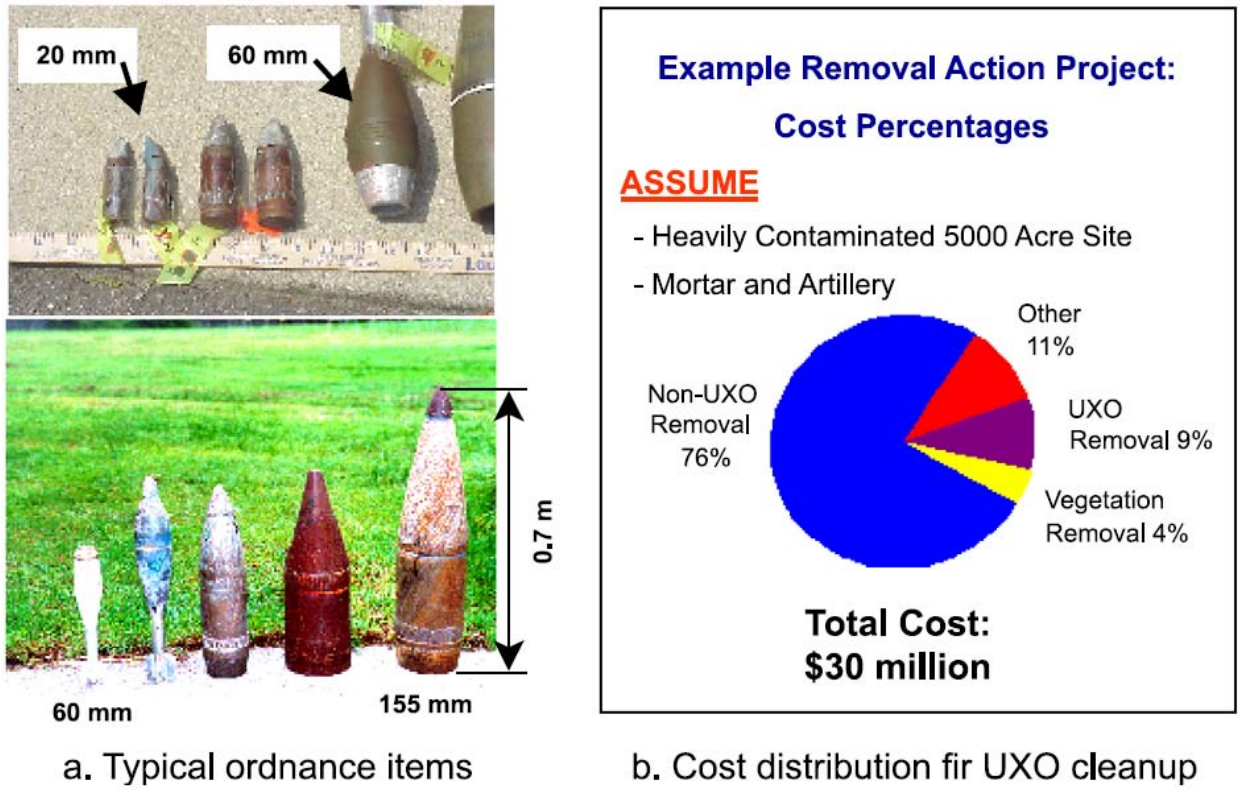

Figure 1: Clean-up costs for a hypothetical UXO removal scenario typical of remediation efforts in the U.S. (after Butler, 2003)

While there has been continued advancement in UXO detection (e.g., Davis et al., 2005), in recent years, research has focused many on developing methods of discriminating UXO from non-UXO items before excavation. Billings et al. (2002), for example, developed an algorithm that automatically fits a dipole-model to each magnetic anomaly and compares the extracted model parameters with a library of UXO items. They found that remnant magnetization was the most effective predictor of UXO, but that some noise anomalies remained indistinguishable from UXO. Gamey (2005) discusses the use of 3D magnetic data and "gradient strings" to improve magnetic discrimination. Sanchez et al. (2006) discuss importance of going beyond a simple dipole model, and suggest discrimination can be improved by the use of higher-order magnetic moments to obtain information about the shape of the anomaly source. A common thread running through these research efforts detection is the difficulty of UXO detection and discrimination in the presence of geologic noise. Butler (2001) summarizes: "Although spatial wavelength filtering might be used for UXO detection in the presence of localized geologic anomalies, UXO detection with magnetometry in a highly cluttered environment will be extremely difficult if not impossible." Considerable effort has been expended characterizing the magnetic signatures of an enormous variety of UXO. We believe that further progress in detection and discrimination depends on developing a similar in-depth understanding of geologic noise.

Models for Geologic Noise

To be effective, both detection and discrimination algorithms require a mathematical model of the background magnetic noise arising from heterogeneities in the magnetic susceptibility of the underlying soil and bedrock. Traditionally, researchers have assumed uncorrelated, uniform random or Gaussian random noise, but this can lead to highly optimistic expectations because natural geologic noise is more complex. Searching for a signal embedded in Gaussian noise is like trying to listen to a conversation while standing close to a hissing steam pipe. The noise is annoying, but different enough from speech that you can still make out the words. Looking for UXO in the presence of geologic noise is much more analogous to trying to follow a conversation in at a crowded cocktail party where you are surrounded by people trying to talk over each other – a much more difficult detection problem because of the similarity between the signal and the noise.

For this pilot project we focused on UXO detection and discrimination using magnetic methods. Magnetics has a long and successful history of application to UXO mapped precisely because in many environments the magnetic signature of UXO, which are largely made of steel, greatly exceeds the magnetic background. This is not true of all sites, particularly those underlain by rock and soils of volcanic origin, for example sites in Hawaii and New Mexico.

Researchers surveying a UXO site in New Mexico reported that over 39% of the magnetic anomalies excavated were not created by UXO, concluding that "localized zones of rock or soil with high magnetic susceptibility ('hot rock/dirt') may have contributed to the high rate of 'no finds'. " (ORNL, 2004).

In a recent SERDP project, Li et al. (2006) went beyond the usual assumption of uncorrelated

random noise. They used a simple model for geologic noise that is Gaussian, but with a power spectrum that decays with wavenumber to create a spatial correlation, and used random changes in phase to generate different noise realizations. They then used optimal Wiener filtering to try to separate UXO from background. This approach to noise simulation is certainly more versatile than random Gaussian, but does not capture either the scaling behavior that is important for wide-area surveys, or an important characteristic of natural variability – zones of low and high noise, or intermittency.

Experience has demonstrated that many geologic processes are scale independent, meaning that geologic properties and patterns appear similar on many scales. For this reason when geologists photograph a rock outcrop they habitually include a rock hammer, lens cap, or some other familiar object for scale (Figure 2), otherwise it is often impossible to distinguish irregularities on the surface of a rock specimen from a surface as large as the lunar landscape. The scale independence of geologic properties has important implications for modeling geologic noise for UXO detection and discrimination in wide area surveys. The implication is that at larger scales, larger natural geologic background anomalies will be more common. The geologic noise information determined from data collected on test site a few hundred meters on a side will not reflect the amplitude variability likely to be encountered when surveying tens or hundreds of square kilometers.

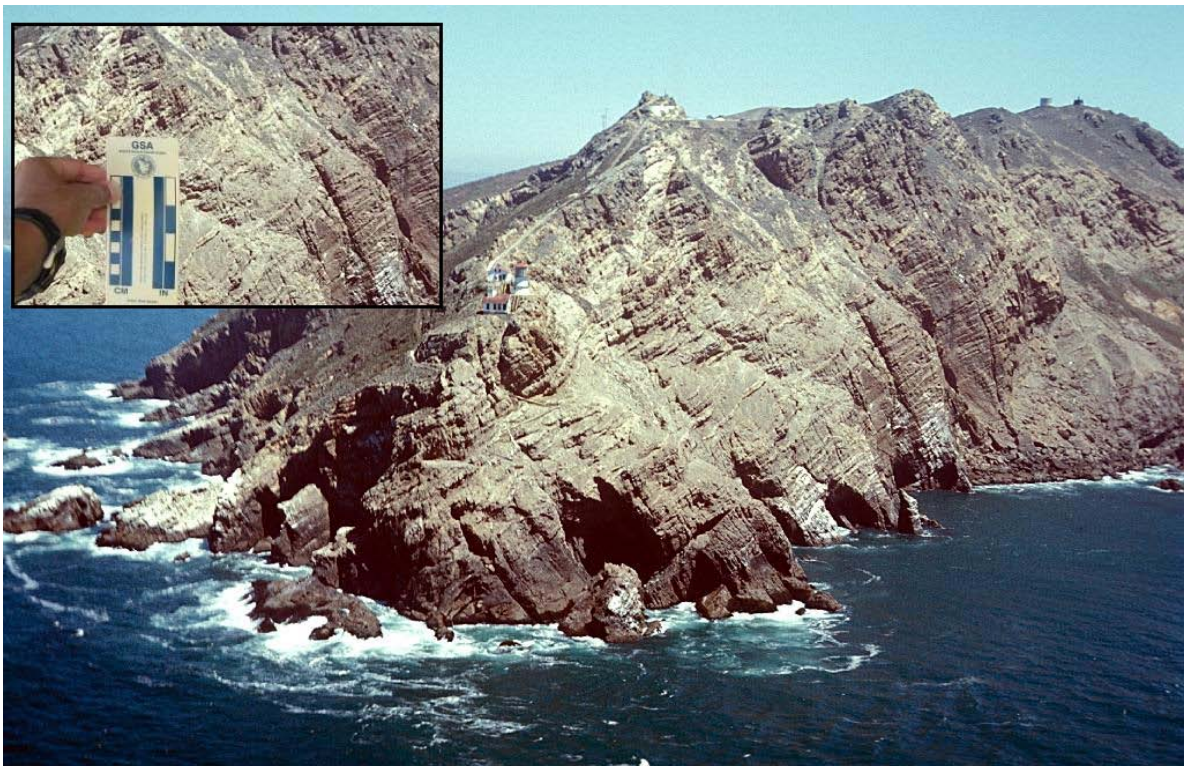

Figure 2: Geologic patterns are often scale independent. Here a false scale on the inset photo (upper left) makes the side of an island appear to be a small rock outcrop.

For wide area assessments,where ultra-low altitude magnetic data are collected over an entire military base or target range, it is particularly important to use a model for geologic noise that are robust at any scale, from sub-meter to tens of kilometers. For this reason, we chose to develop geologic noise models based on multifractals.

Fractals and Multifractals

Fractals can be though of as geometric entities or shapes that are created from a simple mathematical generator that repeats on every scale. A simple example is the Koch snowflake. Starting with an equilateral triangle, we use an algorithm that recursively replaces the central third of each line segment with two smaller segments of equal length pointing outward. Several generations of snowflake are show in Figure 3. When this process is continued indefinitely, the result is a shape has an infinite perimeter and no preferred scale. We can zoom in any number of times on any portion of the snowflake perimeter and we will see the same pattern. What makes fractals more than mere mathematical curiosities is that many elements of nature show this self-similarity over a large range of scales.

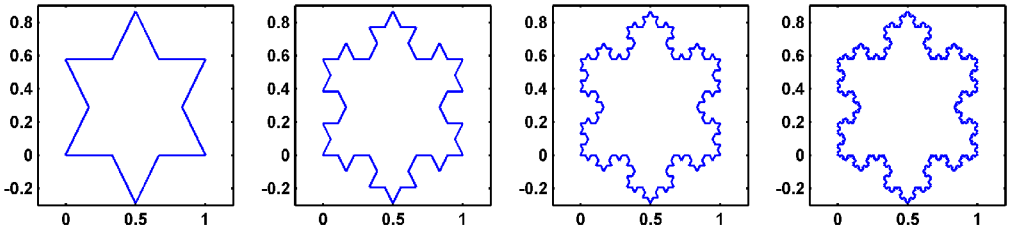

Figure 3: Several interations of the generator for a Koch snowflake.

The concept of a fractal can be generalized from a simple, deterministic, geometric entity such as the Koch Snowflake, to statistical fractals, where is is not the exact shape that repeats on every scale, but the statistical properties that are self-similar (Figure 4). In a classic paper entitled "How long is the coastline of Britain," Mandelbrot discusses how the measurement of something as simple as the distance around an island depends on the length of the ruler. What Mandelbrot found was that there is a direct statistical relationship between the length of the ruler and the total measured coastline. As the ruler becomes smaller, we are able to follow each twist and turn of the coast more precisely and the resulting perimeter grows. Imagine using a ruler so small that you could trace the boundary of each sand grain along the water's edge – the perimeter of Great Britain would be millions of miles! This behavior is like that of the Koch snowflake: there is increasing irregularity as you repeatedly zoom in on the boundary. The self-similarity is statistical rather than geometric, but a fractal model captures many of the features of a coast, and fractal generators can be used to create extremely realistic models of coastlines at whatever scale is required. By starting with different generators, an enormous variety of fractals can be created, and these fractals can be used to generate extremely realistic models of leaves, clouds, landscapes, and other natural objects (Figure 4). Thus, it is reasonable to suppose that a fractal model might also serve as the basis for a scale-independent generator natural magnetic noise. But first we must make one further generalization, from fractal to multifractal.
To model noise requires statistical fractals, but ordinary fractals, which are characterized by a

single fractal dimension, cannot capture a key feature of natural processes – intermittency. When looking at plots of natural magnetic data collected over a large area , it is not uncommon to observe regions that are relatively smooth punctuated by regions of higher amplitude magnetic anomalies. Furthermore, the larger the scale of the data set, the larger the chances of encountering large-amplitude anomalies. Multifractals, unlike ordinary fractals, can capture this punctuated behavior.

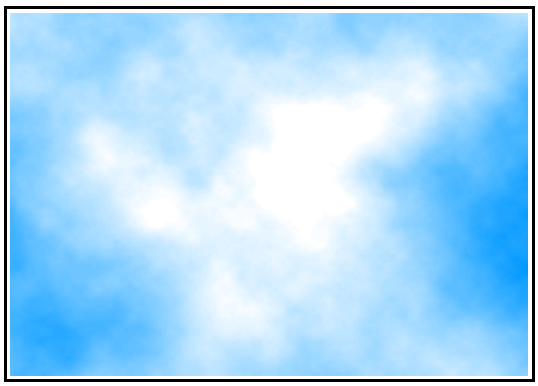

Figure 4. Fractal simulation of a cloud.

A multifractal can be thought of as a a hierarchy of fractal sets each possessing a different fractal dimension that depends on the field's threshold value (Figure 5). This can be made clear with an example. First, it is important to realize that fractals are like regular Euclidean objects; when intersected with a plane, the resulting intersection set has the dimension of the object minus one. Intersecting a sphere (three-dimensional) with a plane results in a disk (two-dimensional). Imagine a fractal representation of land surface elevation (topography). If you slice through the surface at a given elevation (i.e., a horizontal plane), the perimeter of the slice is also fractal, with fractal dimension equal to that of the surface minus one. If the topography were viewed as monofractal of dimension D, then the dimension of the perimeter is D-1, which is independent of the elevation at which you cut the surface. This is not realistic, as one expects the perimeter to be more sparse as the elevation is increased. For a multifractal surface, each perimeter will be fractal but with a different fractal dimension (that decreases with elevation).

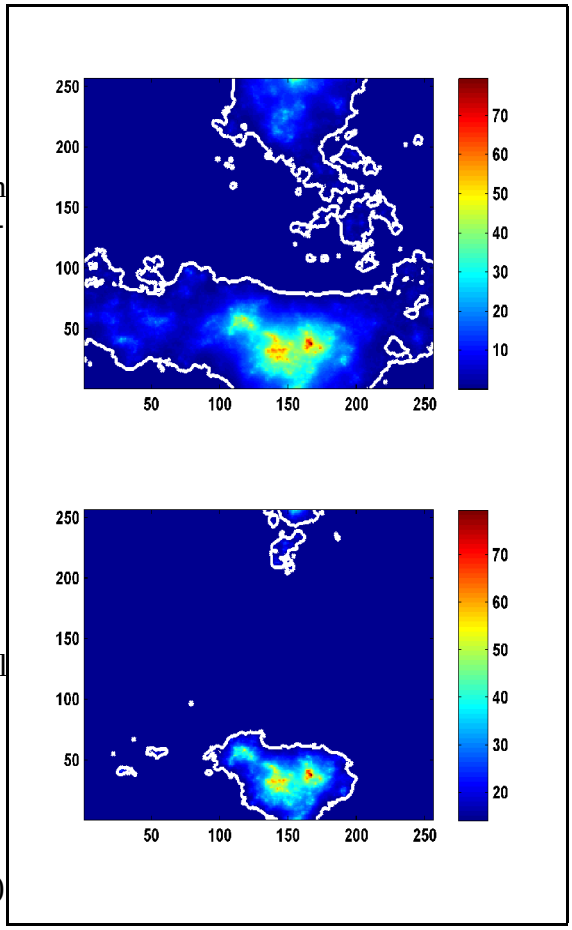

Figure 5. The same fractal cut at different thresholds. For a multifractal the fractal dimension of the perimeter (white line) depends on the threshold, but does not for a monofractal .

The multifractal model is viewed as a means of "distributing" a quantity (e.g., land surface elevation) over space. It has a strong physical basis, arising naturally from the study of turbulence and atmospheric dynamics, modeling the cascading of energy from large eddies into ever smaller ones. In recent years, numerous papers have been published demonstrating that various natural processes ranging from cloud formation, to topography, to earthquake periodicity, can be effectively modeled using

multifractals.

Project Goals

The goal of this project is to investigate the use of multifractals to model the magnetic noise encountered by wide-area aeromagnetic surveys of UXO sites. More realistic models of geologic noise can be used to assist researchers developing detection and discrimination algorithms by creating an electronic proving ground of any size that accurately captures the variability encountered in nature for a wide variety of geologic environments. Multifractal models of geologic noise could then be used to assess the likelihood of false positives and false negatives as a function of the size of the area to be surveyed, the survey parameters, and the geologic environment. In this pilot study we have focused on the multifractal representation of natural variations in magnetic susceptibility. The methods we discuss may be generalized in the future to include other geologic properties, such as electrical conductivity and dielectric permeability, which control the noise levels for time-domain electromagnetics, ground penetrating radar, and other geophysical methods that are employed to map UXO.

Methods

Universal Multifractal Modeling

Fractals belong to the category of scaling models that rely on the fact that the values of the field at different scales are related through a transformation that involves only the scale ratio (i.e., there is no characteristic length scale). Or mathematically,

$$Pr(\Phi_\lambda \geq \lambda^\gamma) \sim \lambda^{-C(\gamma)} \tag{1}$$

where Pr refers to "probability," the tilde means equality within slowly varying constants, and $C(\gamma)$ is the codimension of the field, a function that is non-linear, increasing, and concave with the order of the singularity, γ. Or in plain English, the probability of the multifractal field exceeding the threshold λ^γ at any given scale, λ (meters, kilometers, hundreds of kilometers), is proportional to that scale raised to the codimension $C(\gamma)$, so the larger the scale, the greater the chances of the field exceeding any given threshold, implying that you find more large noise anomalies as you increase the scale of the survey.

Equivalently, we can express the scaling properties in terms of statistical moments (e.g., mean, variance) instead of probabilities:

$$\langle \phi_\lambda^q \rangle \sim \lambda^{K(q)} \tag{2}$$

where $\langle \phi_\lambda^q \rangle$ is the qth moment of the field (with q taking on non-integer values), the angle brackets represent ensemble averages, and $K(q)$ is related to the codimension in a Legendre transform (see Boufadel et al., 2000). Equation 2 states that if we know all of the statistical moments of a multifractal field, this is equivalent to knowing its probability distribution. The computation of moments is easier than computation of the probability distribution from the data.

Scaling properties of a geophysical quantity, G, may be characterized using the structure function (Monin and Yaglom, 1975, Davis et al., 1994; Boufadel et al., 2000):

$$\langle |\Delta G_s| \rangle = \langle |G(x) - G(x+s)|^q \rangle \approx s^{\xi(q)} \quad (3)$$

where s is the spatial lag, the symbol ≈ means proportionality within slowly varying quantities, such as Log(s) (Meneveau and Sreenivasan, 1987), and the angle brackets imply ensemble averages. The statistical behavior of the field is governed by the structure function exponent, $\xi(q)$. Equation (3) generalizes the variogram (q = 2) to include lower and higher order moment. This generalization is needed when the process is multifractal. Equation 3 states that the structure function (e.g., the variogram) is a power law function of the lag (scale). This is key, because it tells us that *if $\xi(q)$ is known at any scale we can fully characterize G at any other scale*.

To determine whether or not a field is scaling, one computes $<\Delta G_s(q)>$ for a certain value of q (say q = 2) as a function of the lag, s, and plots Log($<\Delta G_s(q)>$) versus Log(s). If the result is approximately linear then the quantity G is scaling. The slope of this line yields $\xi(q)$ for the value of q plotted. To distinguish between monofractal and multifractal behavior, the process is repeated for many values of q. One then plots of $\xi(q)$ as a function of q. If $\xi(q)$ varies linearly with q (say up to q < 4) then G is monofractal. If $\xi(q)$ is nonlinear convex (downward facing) then G is multifractal. The structure function, $\xi(q)$, behaves this way because there exists a one-to-one relationship between between $\xi(q)$ as a function of q, and the fractal dimension as a function of threshold D(T) (Frisch and Parisi, 1985; Menevearu and Sreenivasan,1987). Recall that for monofractals D(T) is independent of the threshold value T, hence $\xi(q)$ increases linearly with q, but such is not the case for multifractals. Higher order moments (large values of q) accentuate the role of large values in the field G (higher thresholds), while for smaller values of q, $\xi(q)$ depends primarily on the smaller values of G.

The Fourier power spectral density or simply the spectrum is another tool to assess scaling. A field G is scaling if its Fourier spectrum is power law as function of the wave number, viz:

$$E_G \propto k^{-\beta} \quad (4)$$

where k is the spatial wave number. The field G is called fractal if β is between 1 and 3; this is to allow D(T) to be less than 2 if the data are a one-dimensional series. Such a field is non-stationary and its variogram keeps increasing with the lag distance, s. For β > 3, the field is scaling but not fractal. An example would be the distribution of wave heights at sea as a function of space, where 4 < β < 5 (Phillips, 1985). If β is such that -1 < β < 1, then the field G represents the increments of a fractal field. It is also stationary (Davis et al., 1994), and the variogram of G would exhibit a sill. We are referring to the so-called ‘‘wide-sense stationarity’’, which relates to the behavior of the second order moments, such as the correlation function and the variogram (Yaglom 1987, p56). We believe that the stationarity of the probability distribution function (also known as strict stationarity) is rarely achieved with geophysical data. A more recent classification based on the value of β is the following: if β < 1 the field is conservative, for β > 1 (but still β < 3) the field is nonconservative. Conservative fields have their mean value conserved when the scale of observation is changed.

From an analysis point of view, when $\beta > 1$, the structure function (SF) is a convenient tool for characterizing scaling properties. For fields that are scaling and conservative (i.e., $-1 < \beta < 1$), the SF is not a power law (i.e., the second equality in Eq. 3 is not valid) but the correlation function is a power law at large lags. The correlation function is defined as:

$$R(s) = \langle (G(x) - \bar{G})(G(x+s) - \bar{G}) \rangle \quad (5)$$

where $\bar{G}$ is the average value of the field. Hence, analyzing the field using the SF only might not reveal its scaling properties if $\beta < 1$. Yaglom (1987, p 390) shows that the spectrum is the Fourier transform of R(s) for $\beta < 1$ and the Fourier transform of the SF for $\beta > 1$. For this reason, it is expedient to verify the scaling of a field using the spectrum first. Then depending on the value of β, one could use either the structure function (for $\beta \geq 1$) or singularity analysis (Davis et al., 1996; Boufadel et al., 2000) (for $\beta < 1$) to quantify multifractality.

The discussion above is general and does not depend on the adopted multifractal model. However, the adoption of such a model simplifies the analysis and allows generations of stochastic realizations. We will use for this purpose the universal multifractal model developed by Schertzer and Lovejoy (1987). The Schertzer and Lovejoy (S&L) model is a generalization of the log normal model (Kolmogorov, 1962; Obukhov, 1962; Yaglom, 1966; Monin and Yaglom, 1975, p 614). It relies on using the α-stable family distribution, which is a generalization of the Gaussian distribution, to include, for example, infinite variance distributions. The α-stable distribution depends on four parameters (Grigoriu 1995; Nikias and Shao 1995; Uchaikin and Zolotorev 1999), but in multifractal studies, two of the parameters are fixed (Boufadel et al. 2000). Hence, only two parameters are of interest: α and C_1. The parameter α is such $0 < \alpha \leq 2$, the upper limit being the Gaussian distribution. As α decreases, the frequency of sudden large jumps in the random field increases. The parameter C_1 is known as the scale parameter. It is a measure of the width of the distribution, and is equal to half the variance when $\alpha = 2$. As C_1 increases, the magnitude of the sudden large jumps increases (Boufadel et al. 2000). Studies have shown that the S&L model is flexible in fitting observed data (Lavallée, 1991; Schmitt et al. 1995; Liu and Molz, 1997; Tennekoon et al., 2003). In the S&L model the structure function exponent (Eq. 3) is given by:

$$\xi(q) = qH - \frac{C_1}{(\alpha - 1)}(q^{\alpha} - q) \quad (6)$$

where H is a parameter that is commonly in the range [0,1]. Hence, knowledge of the values of the parameters α, C_1, and H is sufficient to characterize a field and to generate stochastic realizations of the field.

One simple way to generate multifractals is by multiplicative cascades. This approach was originally developed to model turbulent flow, where energy from large eddies is progressively dissipated into smaller and smaller eddies. Figure 6 illustrated the process. Starting with a field that is homogeneous over the entire region interest, the value of the field (magnetic susceptibility in our case) is statistically redistributed to finer scales according to probabilities governed by the selected multifractal parameters. Because the total volume under the curve is conserved, increasingly high peaks develop, separated by regions of small values causing the field to appear sparse at some locations. By judicious selection of model parameters, a wide variety of textures

can be simulated. Figure 6 shows multifractal simulation by discrete cascade, but it is also possible to synthesize continuous multifractals using Fourier methods (Wilson et al, 1991; Pecknold, 1993; Tchiguirinskaia et al., 2000), which is the method we employed in our simulations.

Whether simulated by discrete or continuous cascade, the key is to first use the data to obtain the multifractal parameters α, C_1, and H. We will illustrate how this is done our discussion of our experiments with synthetic data sets. But first we discuss the justification for using multifractals to model magnetic data.

Multifractal Modeling and Magnetic Data

Our choice of fractals as a model for soil and rock properties is motivated by previous works in the field. Pilkington and Todoeschuck (1993) analyzed (in the horizontal direction) magnetic data in Canada using Fourier techniques, and found the spatial power spectrum to decay as $k^{-\beta}$, where β is a real number such that $2 < \beta < 4$. Such a power law behavior evidences scaling regime. These findings were further confirmed by the authors in another publication (Pilkington and Todoeschuck 1995). Maus et al. (1999) conducted variogram analysis on magnetic data in Canada and found the data to exhibit scaling behavior as function of the horizontal distance. Studies in the soil science field have shown that the soil pore structure is fractal (Perrier et al. 1996; Baveye et al. 1998). Scaling behavior has also been noted for subsurface properties (namely the intrinsic permeability, K) as a function of space. (Hewett, 1986; Neuman, 1990; Molz and Boman, 1993, 1995; Painter and Paterson, 1994; Painter 1996, 1998; Molz et al. 1997; Boufadel et al., 2000). Fractality has been found in other geophysical fields, such as river flows (Gupta and Waymire 1990), water in the atmosphere (Davis et al., 1996), carbon content in ice cores (Schmitt et al. 1995), and land topography (Lavallée et al., 1993; Lovejoy et al., 1995).

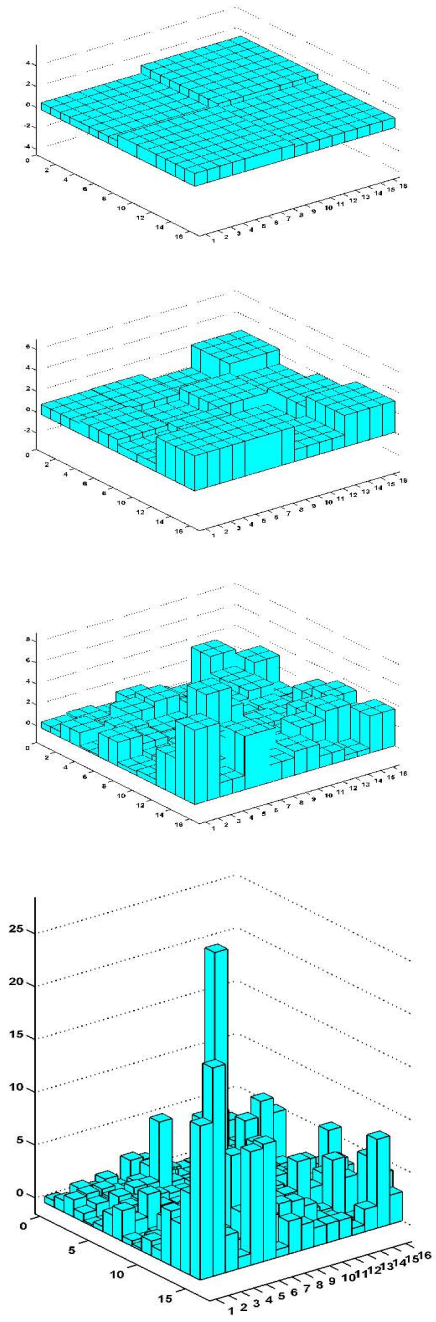

Figure 6. A multifractal cascade starts with a uniform quantity that is stochastically subdivided to ever finer scales while maintaining the ensemble average. Eventually singularities (spikes) and relatively quiet areas develop.

Lovejoy et al. (2001) and Pecknold et al. (2001) published a pair of papers investigating the multifractal modeling of geomagnetic data collected over the Canadian shield. Rather than model the magnetic field directly, they chose to model the underlying magnetic susceptibilities and use their susceptibility models to

generate simulations of the earth's magnetic field. To do this they made a number of assumptions: (1) the magnetization of the geologic material is purely induced, no permanent magnetic moments; (2) the field can be viewed as arising from a stratified earth; (3) that the earth's field can be approximated as vertical (90 degree inclination, a reasonable approximation for Canada).

For this project we also elected to model the magnetic susceptibilities rather than the magnetic field. Because we are not interested in continental scale models, we ignored the deep structures that contribute mainly to extremely large-scale heterogeneities in the magnetic field, and we approximated the near-surface soil and bedrock geology as a single horizontal layer with a multifractal susceptibility distribution.

Experiments with Synthetic Magnetic Data

Before applying universal multifractals to the modeling of magnetic data collected in the field, we tested whether we could create a multifractal magnetic field and then analyze the synthetic data to recover the multifractal parameters uses to generate the synthetic data. The following example illustrates the process for a grid representing an area half a kilometer on a side with a 0.5 m grid spacing.

Generation of a Multifractal Susceptibilities

The generation of multifractal field is described in detail by Tchiguirinskaia et al. (2000), Pecknold et al., (1993) and Wilson et al. (1991). We summarize the steps and refer the reader to these publications for more detail.

Multifractals are generated by a multiplicative cascade, but the same process can be achieved by adding quantities and then exponentiating them at the end. The additive process is called the generator, and for this we used random, negatively-skewed, Lévy noise with the desired α and C_1 values. The noise is then Fourier transformed and fractionally integrated by mutiplying by $|k|^{-d/\alpha'}$ in Fourier space, where $1/\alpha+1/\alpha'=1$. After taking the inverse Fourier transform to return to real space the field is exponentiated to convert the additive process to a multiplicative process. The data are then normalized to create a conservative multifractal field. The data are then Fourier transformed again and fractionally integrated by $|k|^{-H.}$ to obtain the desired universal multifractal with parameters α, C_1, and H. This multifractal field is then scaled to give the desired range of values for the magnetic susceptibilities. Changing the universal multifractal parameters adjusts the smoothness, and intermittency of the resulting multifractal, making it possible to capture a wide range of behaviors while maintaining the fundamental scaling behavior (the statistical nature of the field is the same at every scale). The process is illustrated for a 1-D example in Figure 7.

Simulation the Magnetic Field

To go from the multifractal model of magnetization to the magnetic field, we used a simple horizontal sheet model. This is reasonable given that it is the geologic variability of the shallow soil and bedrock that produces the short-wavelength anomalies can obscure the signature of

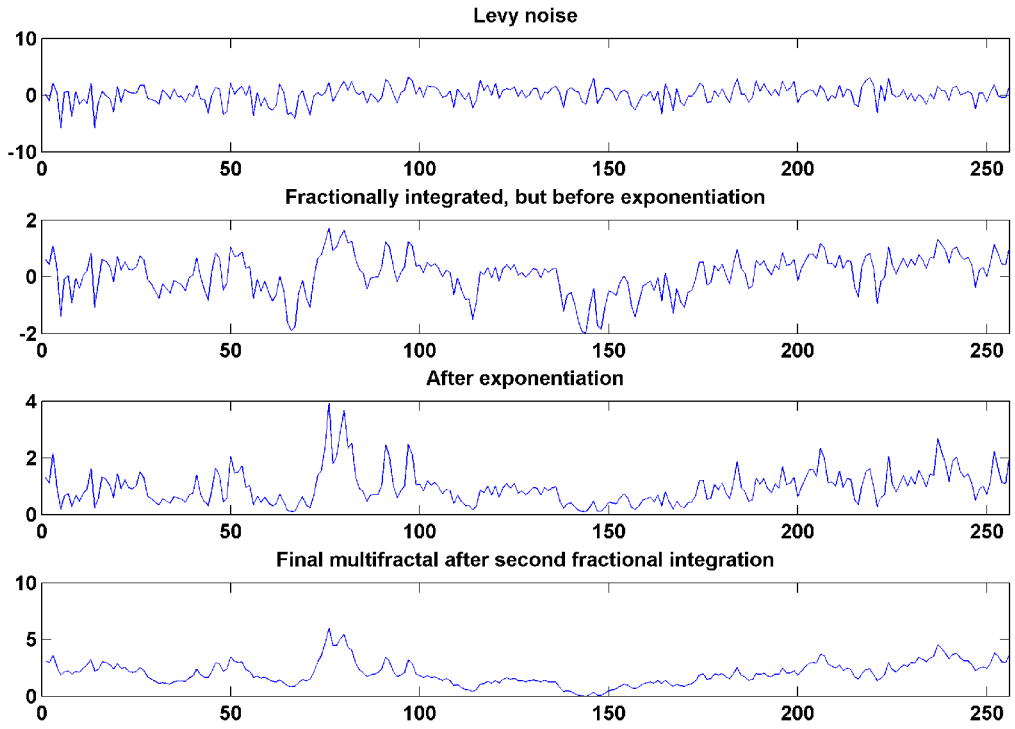

Figure 7: The figure illustrate the creation of a multifractal using Fourier methods for the 1-D case. From top to bottom: Levy noise is generated with the desired α and C_1 values. The noise is converted to an additive process by partial integration in the Fourier domain. The additive process is converted to a multiplicative process by exponentiation after returning to the spatial domain. Finally, a second partial integration in the Fourier domain yields a multifractal with the desired value of H. (α = 1.8, C_1 = 0.5, H = 0.4)

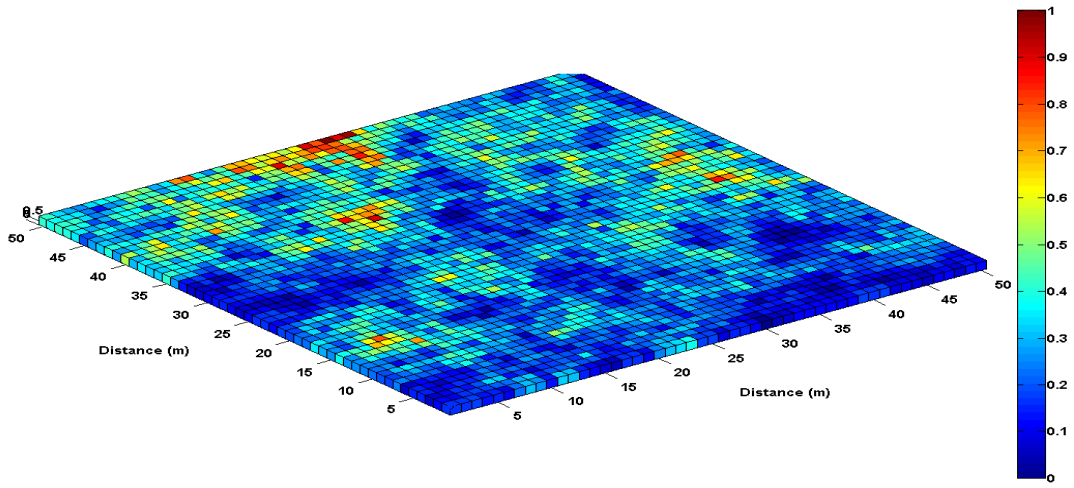

Figure 8: Model for a 0.5 m-thick horizontal layer with 1-m horizontal cells having a multifractal magnetic susceptibility distribution. The susceptibility values here are scaled between 0-1, but can be adjusted to have any desired range.

small UXO targets. For a sheet model the magnetization varies only in the horizontal direction (Figure 8). Assuming purely induced magnetization, the magnetic field at any elevation above ground level can be calculated in the Fourier domain using the equation (Blakely, 1996):

$$F[\Delta T] = F[M]\left\{2\pi C_m \Theta_m \Theta_f e^{(|k|z_0)}\left(e^{-|k|z_1} - e^{-|k|z_2}\right)\right\} \qquad (7)$$
$$z_0 < z_1, z_1 < z_2,$$

where $F[\Delta T]$ is the Fourier transform of the magnetic anomaly, $F[M]$ is the Fourier transform of the magnetization, C_m is a constant (10^{-7} henry/m), Θ_m and Θ_f are the orientation vectors for the magnetization and the earth's field, respectively, *k* is the wavenumber, z_0, is the height above the surface of the measurements, and z_1, z_2, are the depths below the surface to the top and bottom, respectively, of the magnetic layer. The multifractal magnetizations can then be scaled to match the range of amplitudes encountered in the field. Given a multifractal realization of the magnetic susceptibility, the corresponding magnetic field can be calculated at any altitude. Figure 9a shows a simulation of magnetic susceptibilities over a square area 0.5 km on a side with a grid spacing of 0.5 m. Figure 9b shows the resulting magnetic field calculated at a height of 2.0 m assuming an a multifractal layer of magnetic susceptibilities on a grid spacing of 0.5 m created using universal multifractal parameters H=0.3, α = 1.8, and C_1 = 0.050, and assuming an inducing magnetic field with an inclination of 62°, and a declination of 10°. To apply our methodology to field data, we must first demonstrate that we can successfully recover the original multifractal model parameters from the magnetic data for this synthetic example.

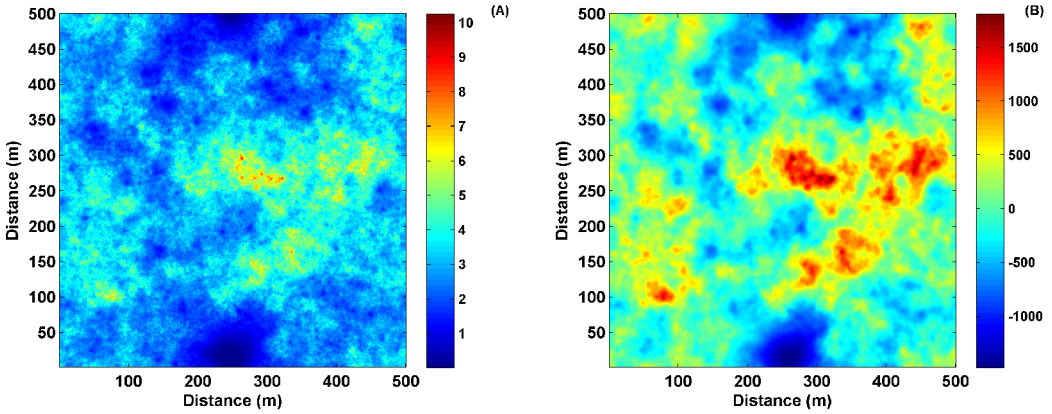

Figure 9: (A) Multifractal distribution of magnetic susceptibilities (S.I.) simulated on a 0.5 m grid. (B) The corresponding total magnetic field calculated at 2 m above the surface (nT).

Recovery of the Universal Multifractal Parameters

We have shown how to produce multifractal distributions of magnetic susceptibilities and then use these to generate a magnetic field, but given a magnetic field, how do we recover the parameterization of of the underlying multifractal distribution? This is the problem we face with field data, so we need to verify that our methodology performs correctly for synthetic data.

Starting with the simulated magnetic data (Figure 9b), the first step is to test that a multifractal model is appropriate by checking that the data are scaling. This we do by checking that a log-log

plot of the Fourier spectrum of the data are linear. A plot of the spectrum of the magnetic susceptibilities is linear (Figure 10), but the Fourier spectrum of the calculated magnetic field clearly is not (Figure 11). This is because the field is calculated at a height of 2 m above ground level to simulate data collection by helicopter, and calculation of the magnetic field at altitudes above the source is equivalent to upward continuation, which is accomplished in the Fourier domain by multiplying by a factor of $e^{-|k|z}$, rendering the spectrum non-linear by preferentially attenuating the higher frequencies. The obvious remedy is to downward continue the data back to ground level by multiplying by $e^{|k|z}$ in the Fourier domain. Upward continuation is stable, because multiplication by a negative exponential is a smoothing operation. Downward continuation, however, involves multiplication by a positive exponential, and is notoriously unstable. Any noise present in the data, even numerical noise, is magnified exponentially by the downward continuation filter. Traditionally, the way around this is to first low-pass filter the magnetic data before downward continuing it, but low-pass filtering will strongly alter the underlying spectrum.

A recent paper by Xu et al. (2007) proposed a new approach to downward continuation that is numerically stable, and dispenses with low-pass filtering at the expense of additional computational time. The idea is straightforward; the magnetic field at the measurement elevation is used as an initial guess for the magnetic field at the ground level, then upward continued (stable operation) and compared with the measured data. The field at the ground level is then iteratively adjusted until the upward continued field and the measured data agree within an acceptable tolerance. Using this approach to downward continuation, no spurious high frequencies are introduced. Figure 12 shows the spectrum of the downward continued magnetic data, which is clearly linear with the same slope as the spectrum of the simulated magnetic susceptibilities, except at the highest frequencies where information was lost through the original upward continuation operation.

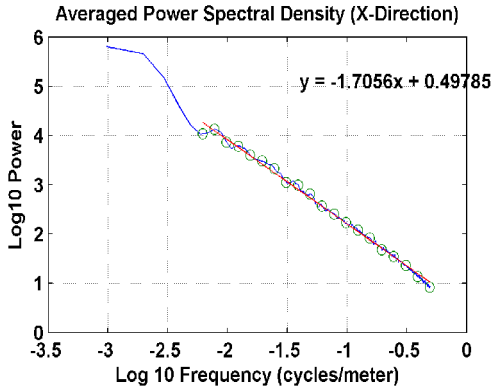

Figure 10: Fourier power spectrum of the simulated magnetic susceptibilities.

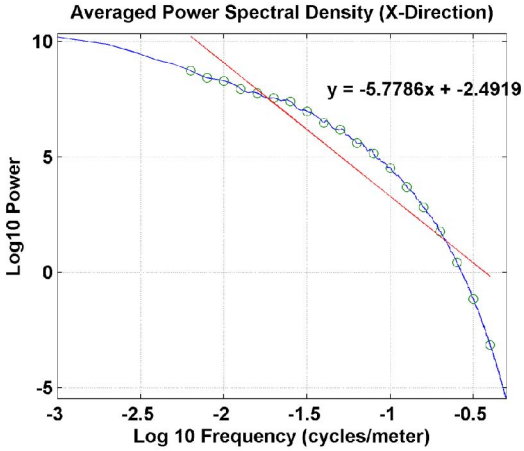

Figure 11: Fourier power spectrum of magnetic field at a flight height of 2 m

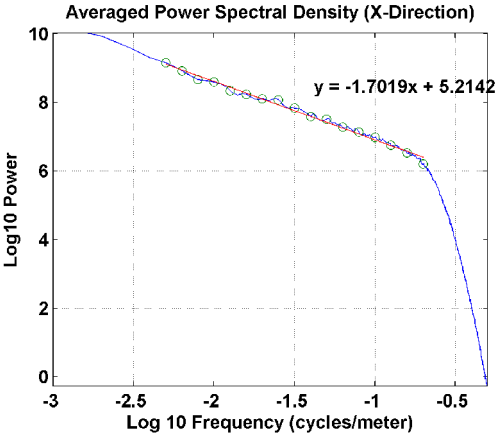

Figure 12: Fourier spectrum of magnetic data downward continued to the surface. above the surface.

The Fourier spectrum of the downward continued magnetic data shows that the underlying magnetic susceptibilities are scaling, therefore a fractal model is appropriate. Thus, the first step in analyzing field data will be to downward continue the data and check the Fourier spectrum.

After determining the data are scaling, the next step is to find the corresponding universal multifractal parameters α, C_1, and H. For a conservative field (H=0), the structure function (Eq. 6) becomes:

$$\xi_{con}(q) = K(q) = \frac{-C_1}{(\alpha-1)}(q^{\alpha}-q). \tag{8}$$

The parameters α, C_1 can be estimated using the double trace moment method (DTM) (Lavallée et al, 1992, 1993; Boufadel et al., 2000). In this technique the data are first raised to a power η, then averaged over a scale λ (the term "dressed" is often used in the literature). The resulting field will have the moment scaling function, K(q,η) for a universal multifractal given by:

$$K(q,\eta) = \eta^{\alpha} K(q) = \eta^{\alpha} \frac{C_1}{(\alpha-1)}(q^{\alpha}-q), \quad \alpha \neq 1. \tag{9}$$

We obtain an estimate of K(q,η) from the data using Eq. 3 to calculate the q^{th} moment, for the data averaged using different values of η. The slope of a log-log plot of K(q,η) versus η yields an estimate of the parameter α. Using different values of q should yield parallel lines with the same slope, serving as a check on the α estimate. Given α, we can deduce C_1 from same plot from the value of K(q,η) at η = 1 and Eq. 9. There is one caveat. The process breaks down in practice for higher order moments (typically, q > 4) where one or two high data values dominate the ensemble averages, and can also break down for extremely low values of q due to noise or discretization error (Pecknold et al., 2001). Avoiding these extremes, the DTM technique yields good estimates of α and C_1.

For a non-conservative field (H > 0), one has a third parameter to estimate, H. The DTM technique applied to non-conservative field yields incorrect values for α and C_1. If the value of H were known, one could convert the non-conservative field into a conservative one by fractional differentiation of order H (equivalent to multiplying by k^H in Fourier space, where k is the wavenumber). Not knowing the value of H, we employ a "bootstrap method." We take the increment of the data (which is equivalent to fractionally differentiating by assuming H = 1), and use the DTM to estimate α and C_1. The DTM technique will yield reasonable estimates as long as H < 1. For a conservative field, the slope, β_{con} , of a line fitted to a log-log plot of the Fourier power spectrum is:

$$\beta_{con} = 1 - K(2), \tag{10}$$

where K(q) is given by Eq. 9. Using the values for α and C_1 obtained from the DTM results for the differenced data, we then calculate β_{con} and compare with the β value obtained from the power spectrum of the original data. The value of H can then be estimated as:

$$H = \frac{\beta - \beta_{con}}{2}. \qquad (11)$$

This value of H is then used to fractionally differentiate the original data, the DTM technique applied again to obtain new estimates of α and C_1, a new value of H obtained from Eq. 11, and the whole process repeated until the parameter estimates converge (Pecknold et al., 2001), usually within a few iterations. Applying this method to the downward continued magnetic data in our example, we obtain parameter values of H=0.4, α = 1.7, and C_1 = 0.059, which are quite close to the parameters used to generate the multifractal magnetic susceptibilities (H=0.3, α = 1.8, and C_1 = 0.050). Thus, we have described a procedure for fitting a universal multifractal model to total field airborne magnetic data and generating new realizations with the same statistical behavior at scales both smaller and larger than the original data set. We will now apply the methodology to several field data examples.

Case Histories of Multifractal Simulation of Field Data

We evaluated our methodology using three different test sites representing low, medium, and high levels of geologic noise relative to the magnetic signal strength of buried UXO. For the low-noise case we selected the Sierra Army Depot in California. For the medium-noise site we selected Fort Ord, California, and for the high-noise site we selected Isleta Pueblo, New Mexico. We will present the case histories in order of a increasing geologic noise.

Case History: Sierra Army Depot, CA – Minimal Geologic Noise

The Sierra Army Depot is located in southern California, just across the border from Reno, Nevada. A team from Oak Ridge National Laboratory conducted an airborne geophysical survey in January and February of 2003, surveying the Honey Lake area (3466 acres), and the East Shore (1168 acres) using the helicopter-based ORAGS™ Arrowhead system (Figure 13) which is comprised of a linear array of eight Scintrex™ Cesium vapor magnetometers (ORNL, 2003) spacing 1.75 m apart such that each pass cuts a swath just over 12 m wide. The surveys were flown at an average flight height of 1.75 m above ground level for Honey Lake, and 2.21m for the East Shore.

Figure 13: The ORNL Arrowhead system in flight at SIERRA Army Depot.

According to California Groundwater Bulletin 118 (California, 2003), the bedrock under the Honey Valley Basin consists of Plio-Pleistocene and Pleistocene age basalt flow, which are likely to be highly magnetic, but these flows are overlain by lake and near-shore sediment deposits up to 213 m (700 ft) thick. Comprised of sand, clay, and silt, these non-magnetic overlying sediments provide a large separation between near-surface UXO targets and magnetic bedrock.

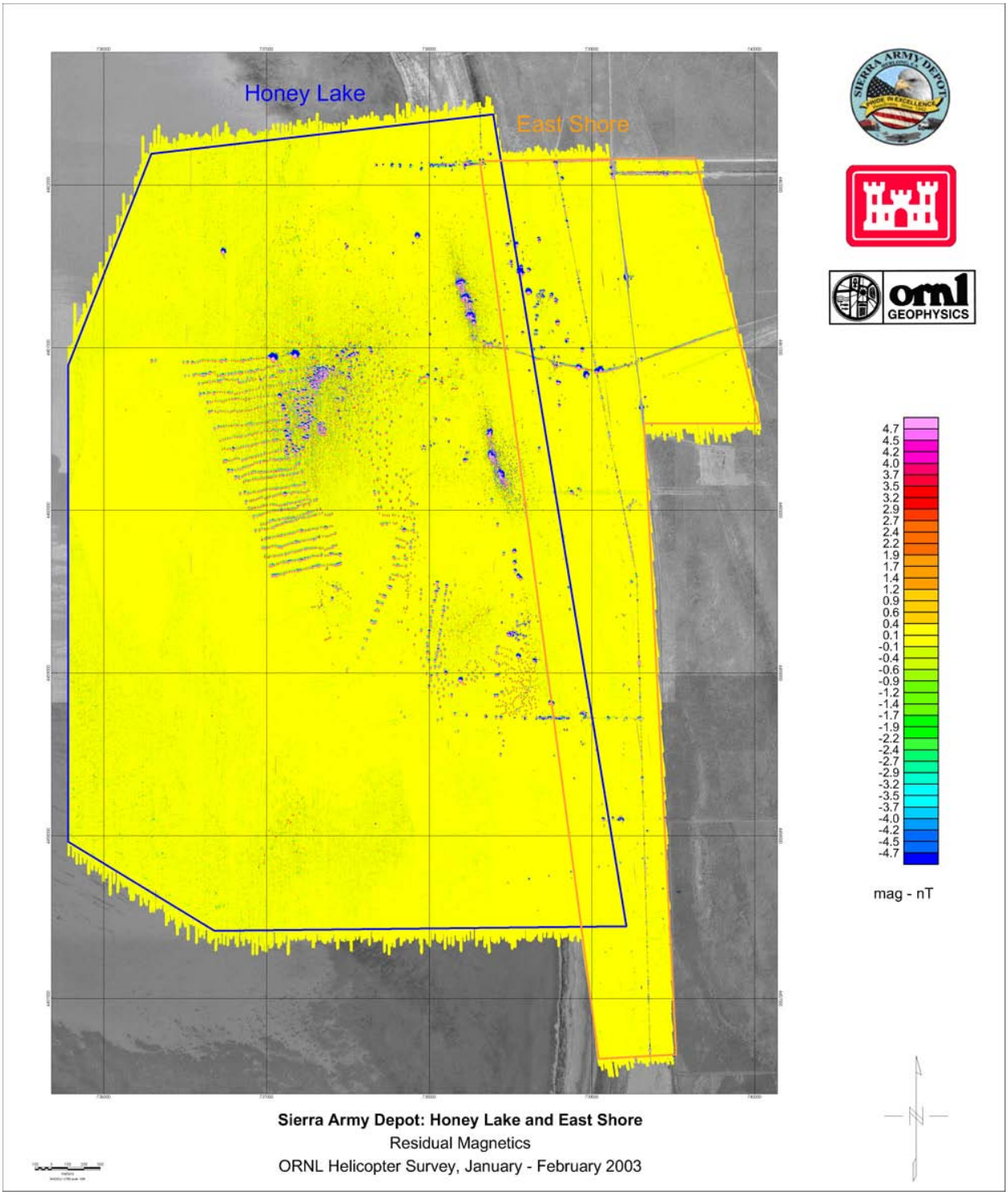

Figure 14: Residual magnetic data from SIERRA Army Depot. Notice the scale. The background magnetic variation away from the UXO is only a few nT (from ORNL, 2003).

The result is a site with virtually no magnetic noise originating from near-surface geologic sources. Figure 14 shows the residual total magnetic field after removing the regional N-S trend. Notice that the background away from the UXO anomalies varies by at most a few nanotesla. This level of compensation for helicopter-related noise sources (rotor noise, flight level fluctuations, GPS time lag, tilt-roll-yaw, heading error, etc.) is far easier to achieve for residual magnetic data then for total field. High-pass filtering down the lines followed by adjustments to bring each trace to zero mean eliminates most of the compensation error. Unfortunately, it also distorts the frequency content of any remaining geologic noise, making it impossible to apply the multifractal methodology.

We analyzed a subset of the ORNL magnetic data, selecting a region with as few UXO anomalies as possible to characterize the geologic background without interference, and attempted to reprocess the total field data to recover the geologic background. Figure 15 shows the total field data for our 1-km test area is dominated by a N-S trend created by deep-seated magnetic sources. After removing the regional N-S trend by fitting and subtracting a second order polynomial surface the magnetic "background" was dominated by small amounts of line-to-line compensation error (rotor, elevation fluctuations, etc.), which masks any anomalies created shallow magnetic rock or soil. It is possible that geologic noise of less roughly 10-15nT is present, but further reducing the compensation error would require microleveling the flight lines. This would require data from E-W tie lines, which were not collected.

We conclude that at sites such as SIERRA Army Depot, where the geologic background is minimal, further improvement in magnetic detection and discrimination will come with reduction in system noise, not synthetic modeling of the magnetic signature of the geology. As we shall see, this is not the case for our two remaining case histories.

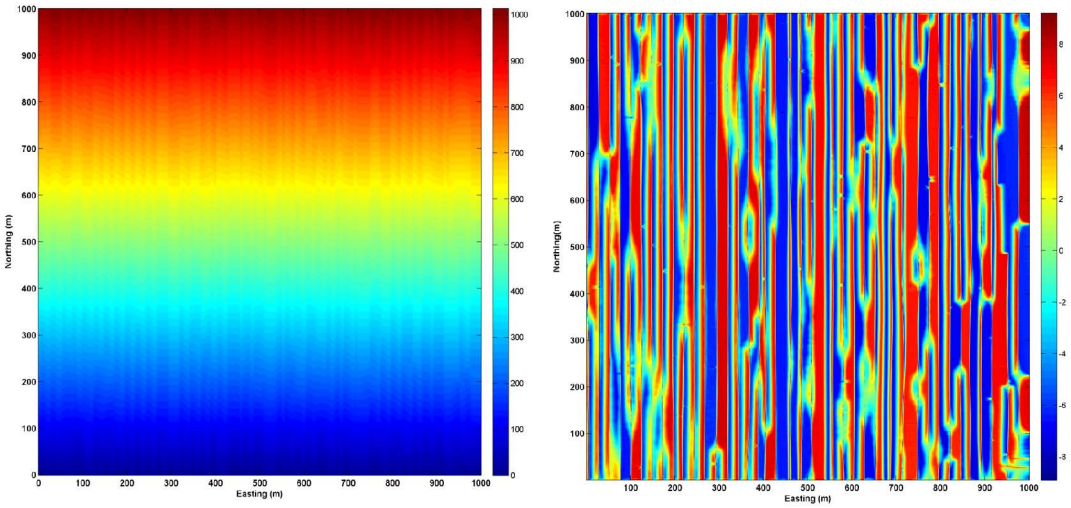

Figure 15: (Left) The total magnetic field for a 1-km test portion of the Sierra Army Depot magnetic data is dominated by a N-S trend created by deep-seated geologic sources. (Right) With the trend removed line-to-line residual compensation error dominates. Shallow geologic sources are too weak to identify. Color scale is in nT.

Case History: Fort Ord, CA – Moderate Geologic Noise

Fort Ord is situated near Monterey Bay, California, roughly 130 km (80 miles) from San Francisco, and close to the Pacific coast. The base was officially closed in September, 1994, however remediation activities continue at the site, including the identification and removal of UXO. In 2005, the ORNL team conducted both helicopter magnetic and electromagnetic surveys of approximately 1,281 hectares (3166 acres) of Fort Ord looking for clusters of anomalies associated with targets and ranges (ORNL, 2005).

Figure 16: ORNL Arrowhead system in operation at Fort Ord. Notice the ridge and trough topography, which is apparently correlated with the anisotropic magnetic background.

The geology is comprised of mesozoic granite and metamorphic rocks overlain by younger alluvial fan, lake, and fluvial deposits (Fort Ord Primer, 2008). Consequently we would expect the bedrock to be magnetic, but the overlying sediments to be non-magnetic, as we saw was the case for the Sierra Army Depot. Magnetic susceptibility measurements the ORNL team on grab samples of the surface sediments confirmed that the overlying sands are non-magnetic. And, as at are Sierra, the Fort Ord magnetic data are dominated by a N-S trend probably associated with the underlying bedrock. Apart from some magnetic background associated with debris, the researchers noted, "Numerous other moderate amplitude responses exist within the survey area, but these are likely more geologic in origin." (ORNL, 2005) These sinuous anomalies appear to coincide with Fort Ord's ridges and trough topography (Figure 16). ORNL researchers speculated that magnetic sediments may have washed down from the nearby mountain ranges can accumulated in the troughs (personal communication, 2008), although confirmation of this hypothesis would require ground follow-up.

Multifractal analysis of the Fort Ord magnetic data was complicated by two factors in addition to the aforementioned anisotropy. First, vegetation coupled with the uneven terrain made flying close to the ground more difficult here than at Sierra Army Depot. The average flight height at Sierra was less than 2.0 m above ground level; at Fort Ord it was 3.5 m. The magnetic response from a small, localized source falls off with the cube of distance, so nearly doubling the flight height means a factor of eight loss in sensitivity. More importantly for the multifractal analysis, it means an increase in the smallest scale that can be resolved. The second challenge in analyzing these data was the survey design. To economize, the ORNL team flew every other line. The Arrowhead system (Figure 16) records data at a rate of 120 data points per second from eight magnetometers spaced 1.7 m apart perpendicular to the flight direction. Flying over Ford Ord at an average speed of roughly 20 m/s, resulted in an extremely fine down-the-line sampling interval of less than 20 cm for lines spaced 1.7 m apart. But by skipping every other line the final result was a data set alternating eight tightly spaced lines with 12 m gaps between the line groups (Figure 17).

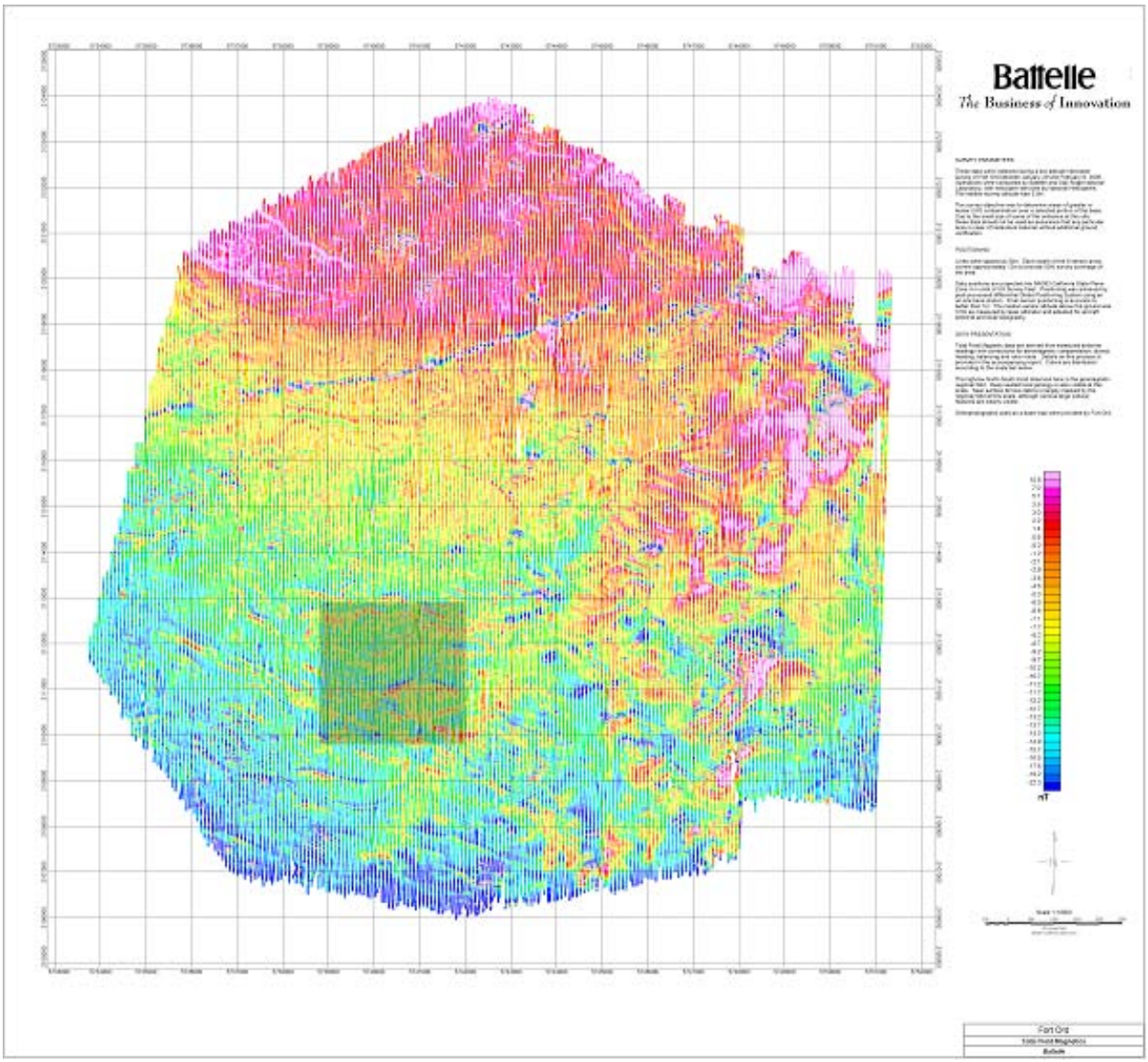

Figure 17: Residual total magnetic field from Fort Ord. Notice the strong N-S trend from deep-seated sources, the 12-m gaps created by flying every other line, and the strong, sinuous anisotropy created by near-surface geologic sources. (From ORNL, 2005). Note: Units for this map are in State Plane feet; each grid cell is 1000 ft on a side. Consequently, the test area is roughly 3x3 cells and is shown as a shaded region above.

Multifractal analysis of the Fort Ord data began with the selection a 1 km^2 subset of the data with a minimum of UXO and other anthropogenic magnetic anomalies. Figure 18 shows the test area in more detail, scaled to emphasize the magnetic background. Even in this relatively clean potion of the Fort Ord data set the few UXO items present produced by far the largest anomalies. Fortunately for our goal of background estimation, the larger UXO items contributed to only a small portion of the test area data, and after clipping the UXO anomaly peaks they contributed negligibly to the power spectrum. The contribution of smaller UXO items that buried in the

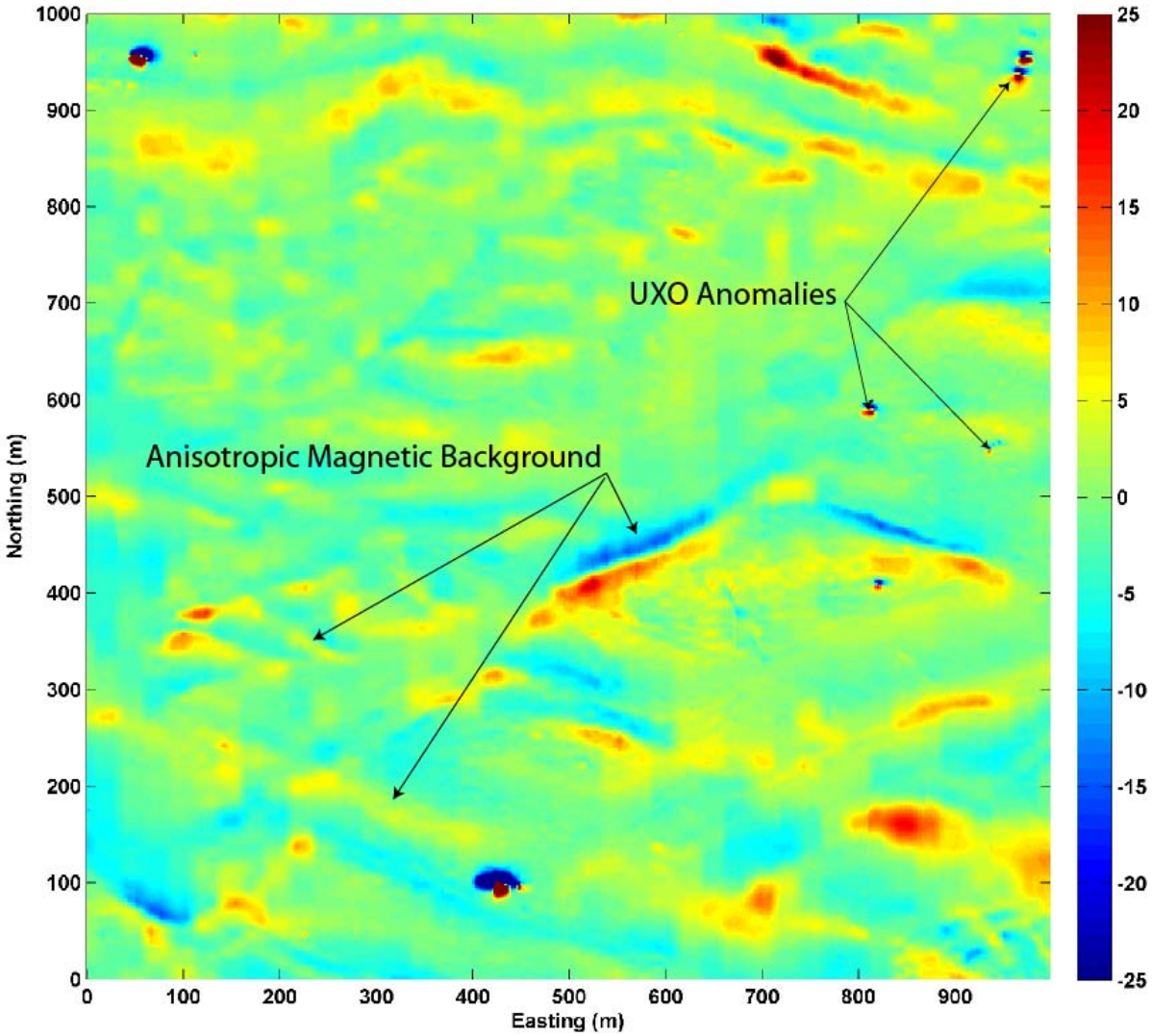

Figure 18: Total field magnetic data for 1 sq km test area selected from the Fort Ord data set (see Fig. 17) as a region with minimal UXO. Although some UXO are present, the anisotropic magnetic background is dominant for most of this region. (Color scale is in nT)

background noise, however, is uncertain. In the analysis that follows we implicitly assume that the sinuous, anisotropic anomalies presumably associated with magnetic sediments dominate. Note that for this test area the data have been interpolated to a 2-m grid, including interpolation across the data gaps created by the alternating flight lines, which may affect the information and the shortest wavelengths, but was unavoidable in this case.

The second step in the multifractal analysis, after selecting a relatively clean subset of the data, is to downward continue the data to the ground surface, then examine the Fourier power spectrum (Figure 19). The result clearly shows fractal scaling (linear decrease with frequency) except for the highest frequencies, which cannot be fully restored by downward continuation. Following the methodology described earlier, we now calculate the double trace moment to determine the

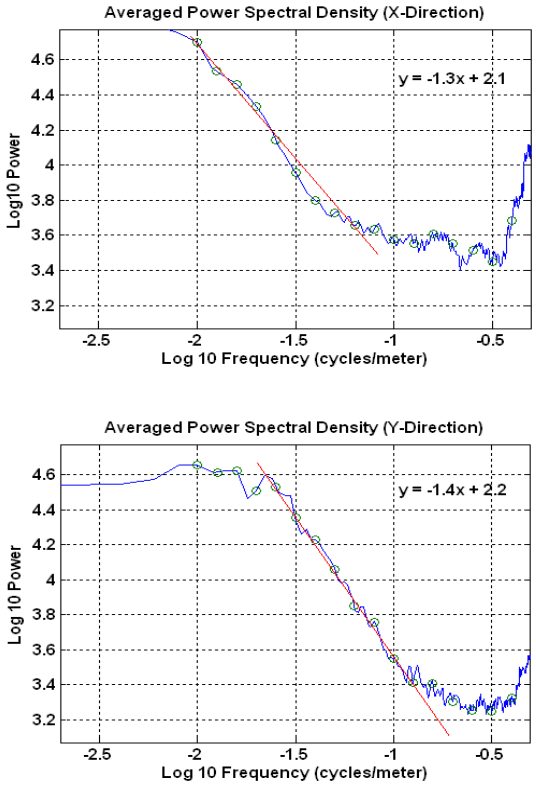

Figure 19: Power spectrum for the 1 sq. km subset of the Fort Ord magnetic data. The linear decrease of the logarithm of the spectrum with the logarithm of frequency is evidence of fractal scaling. Linearity breaks down at the highest frequencies, which cannot be accurately restored by downward continuation.

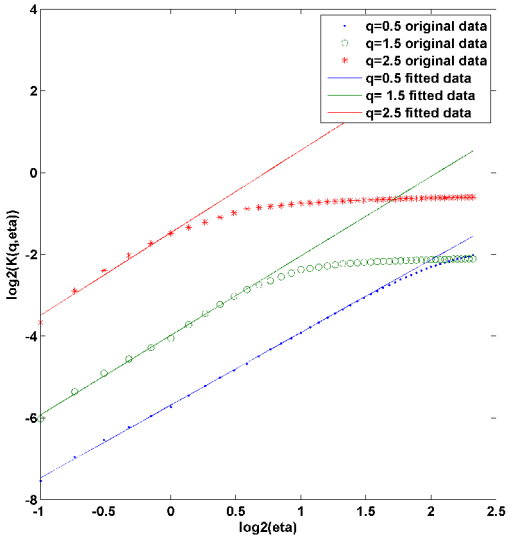

Figure 20: The double trace moment method applied to the data for various moments, q, recovers two of three required universal multifractal parameters: alpha and c1.

universal multifractal parameters (Figure 20). The fits show the expected departure from linearity (divergence of the moments) for high values of η (from Eq. 9). The parallel linear slopes for different values of q, however, lends confidence to the obtained values of $\alpha = 1.8$ and c1 = 0.08. The value of H obtained as described in the methods section was H=0.3.

We now have the parameters required to simulate the magnetic background. However, the simulation methodology assumes isotropy, which is clearly a poor assumption for this site. We have recently begun exploring methods for incorporating anisotropy in our simulations, though this goes beyond the original scope of this pilot project. One straightforward though not very general approach to simulating anisotropy is to use different values for H_x and H_y in the final fractional integration that converts the conservative multifractal into an non-conservative multifractal (means varies with scale). Figure 21a shows the magnetic data from our test area compared with one realization of an isotropic simulation (Figure 21b) using the fitted universal multifractal parameters, and two anisotropic (Figure 21c,d) realizations using anisotropic

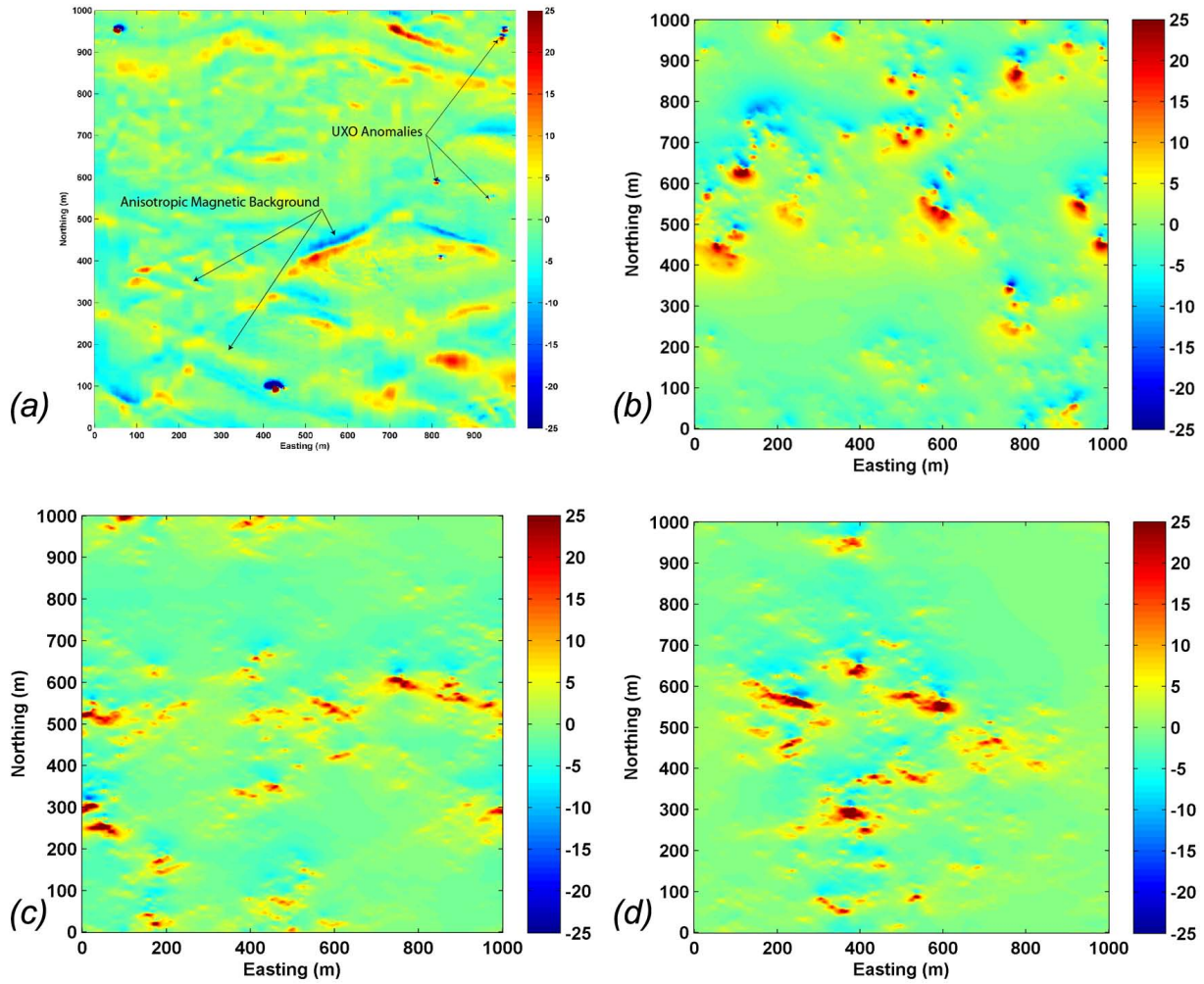

Figure 21: (a) Subset of the Fort Ord total field magnetic data; (b) Isotropic multifractal simulation using the fitted parameters (see text); (c & d) Anisotropic multifractal simulations. Color scale is in nT.

fractional integration, with the parameters selected by eye to achieve a reasonable match.

We conclude from this case history that the magnetic background at Fort Ord is anisotropic multifractal, and reasonable simulations can be achieved with a simple modification to the simulation of isotropic universal multifractals. However, the ad hoc nature of this anisotropic simulation is unsatisfying. A more general approach to the characterization and simulation of anisotropic universal multifractals is possible (e.g., Cheng, 2004; Lewis, 1999; Lovejoy et al., 2001), which can incorporate both anisotropic stratification as well as change in the direction of anisotropy (rotation) with scale, and this will be the subject of our future investigations. Nonetheless, our simple anisotropic model has produced quite reasonable simulations of the magnetic background at Fort Ord.

Case History: Pueblo of Isleta, NM – Strong Geologic Noise

The Pueblo of Isleta is located near Albuquerque, New Mexico. Established in the 1300's, the Native American settlement comprises now Oraibi and Chicale. Over the years portions of this land have been contaminated with UXO by DoD training missions. Researchers from both ORNL and the Naval Research Laboratory have conducted separate demonstrations wide-area assessment at the S1 target area using of ultra-low airborne magnetic mapping. From the point of view of flight logistics, the site is ideal – flat with minimal vegetation (Figure 22) – but still represents a difficult challenge for magnetic detection and discrimination of UXO because of the strong magnetic background. The surface material is thin veneer of Holocene and Pleistocene alluvial and colluvial deposits, which are probably only moderately magnetic, but are underlain by a series of ancient basalt flows which are highly magnetic. Quoting from an ORNL report (ORNL, 2003):

Figure 22: The MTADS airborne system deployed at Pueblo of Isleta, NM. The flat terrain and minimal vegetation made it possible to survey this site with average flight heights below 2 m (Nelson et al., 2003).

> "39% of the ORAGS detections that were dug in S-01 were classed as 'no finds.' This value is high in comparison to other surveys where more standard field excavation techniques were used (for example, <3% at BBR, Van et al., 2004). This number is artificially high in part because excavation radii did not go beyond 1m. One meter is approximately the average separation between the excavated items and their predicted location based on ORAGS-Arrowhead data. Other factors, including localized zones of rock or soil with high magnetic susceptibility ('hot rock/dirt') may have contributed to the high rate of 'no finds' in area S-01."

Similarly, the NRL survey report (Nelson et al., 2003) reports in their results table instances of "target lost in the geology." Thus, magnetic noise was a major problem for these surveys.

The sheer density of UXO items at the S1 site also presented a challenge for our multifractal analysis, making it difficult to distinguish the geologic background (Figure 23). Again, we selected a portion of the dataset away from the main target area, but even for this subset, the magnetic signatures of the larger UXO present dominated the data (Figure 24a). Consequently, we used UXOLab **(**UBC, 2008**)** to model and remove the effect of the 35 largest dipole anomalies, clearly too large and too localized to be of geologic origin. Our multifractal characterization of the residual assumes that the remaining magnetic field is dominated by the geologic noise, even though many smaller UXO items remain (Figure 24b). Ideally for our purposes, the contractor would collect background data in the same geologic setting away from UXO-contaminated sites. Absent uncontaminated background data, we proceeded with our analysis, recognizing that the resulting multifractal simulation will tend to overestimate the

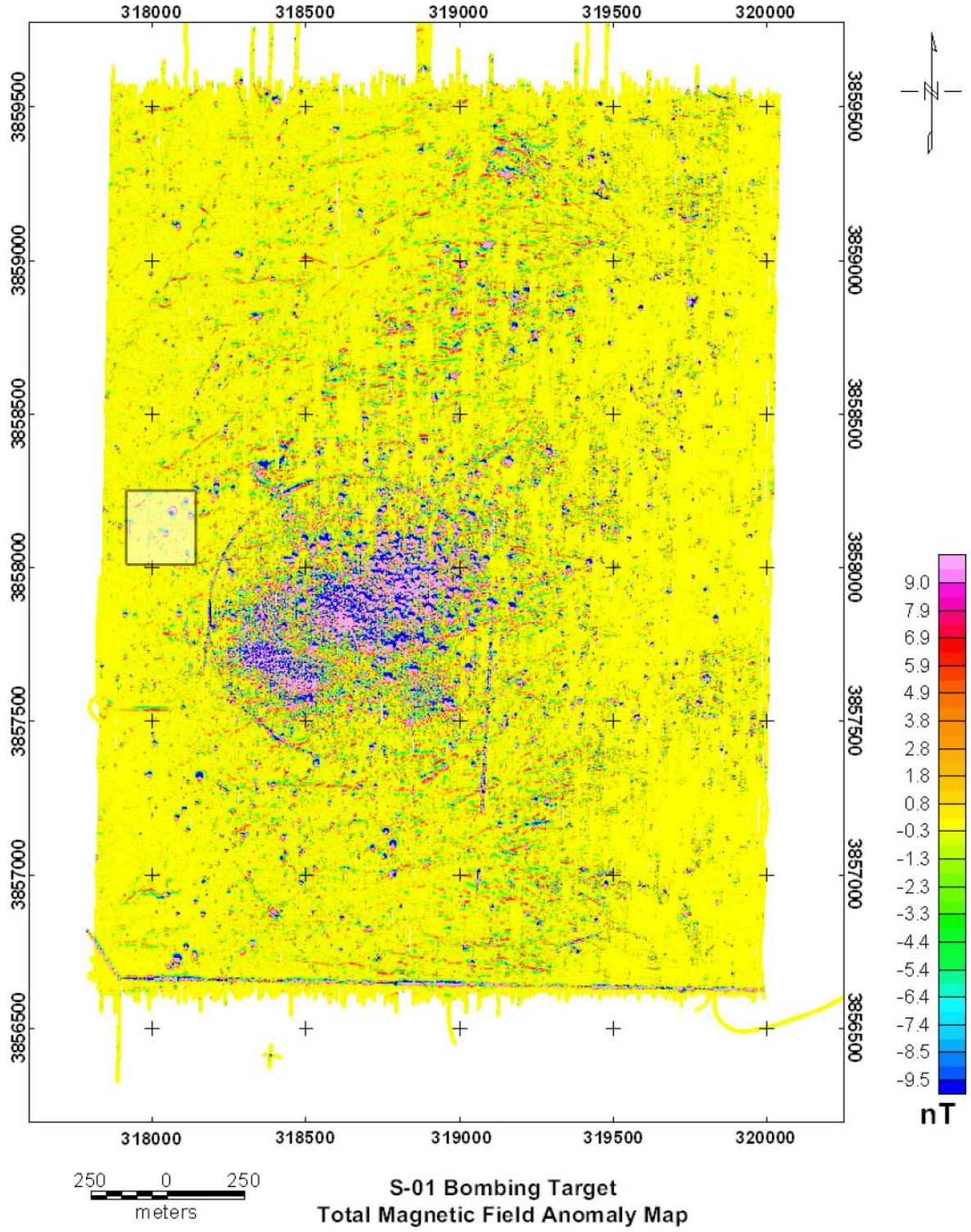

Figure 23: Residual magnetic data for Pueblo of Isleta (ORNL, 2003). Shaded box shows the area selected for multifractal analysis.

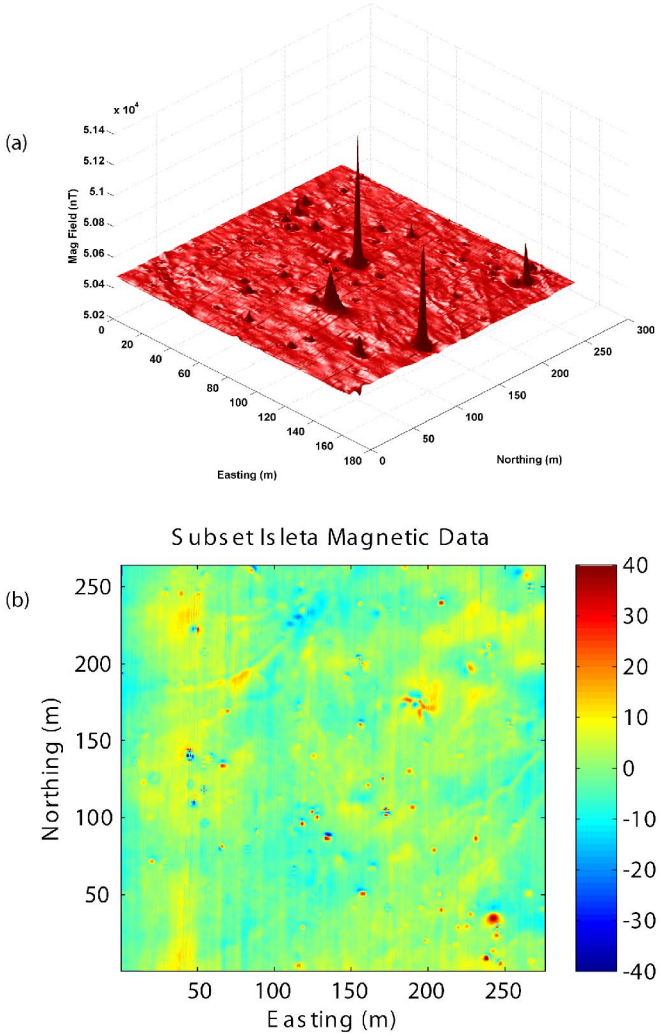

Figure 24: (a) Surface plot of the subset of the Isleta magnetic data (boxed area in Fig. 22) demonstrates that even away from the S-01 target UXO dominates the total magnetic field. (b) The same data with the 35 largest dipole anomalies modeled and removed. Smaller UXO items remain, but now the magnetic of geologic background is apparent. N-S banding is line-to-line leveling error.

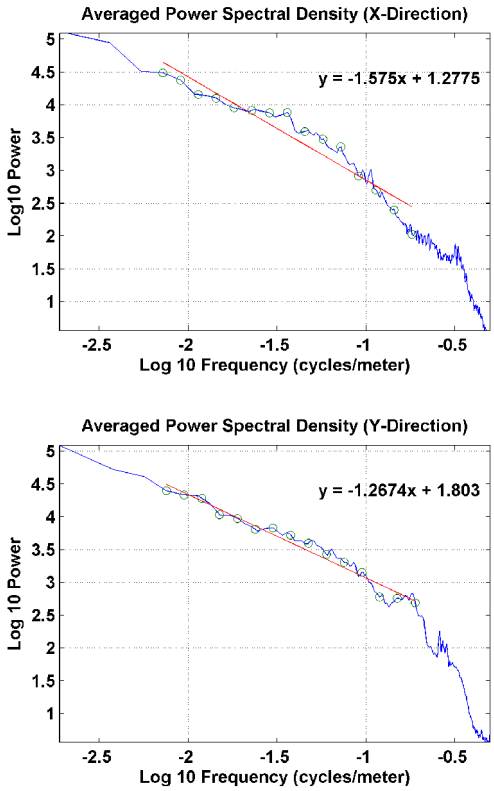

Figure 25: Power spectra of the data subset show scaling except beyond the fitting range where downward continuation has affected the highest frequencies.

number of background spikes (largely affecting the c1 parameter). We will return to this point this point in our summary discussion at the end. The Fourier power spectra (Figure 25) of this subset of the Isleta data show evidence of fractal scaling, though the spectra depart from linear at the highest frequencies, where downward continuation of the aerial magnetic data could properly recover spectral energies. We placed more credence in the spectrum for the Y-direction as the X-direction spectrum also has some contamination by line-to-line leveling error.

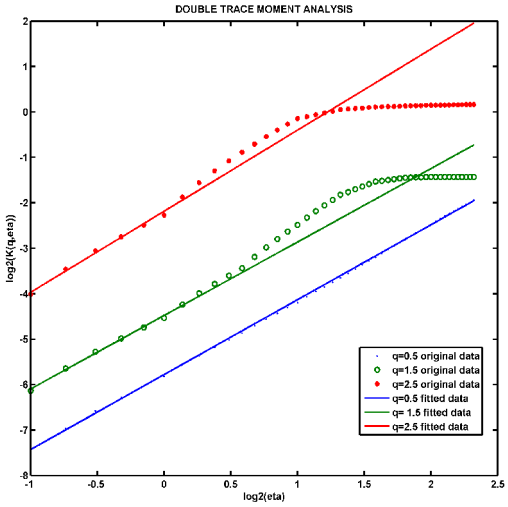

Figure 26: Double trace moment method applied to the Isleta test area data.

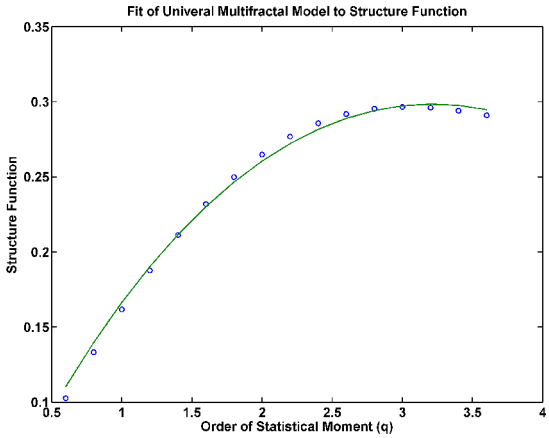

Figure 27: Direct fitting of the structure function (Eq. 6). The concave downward curvature is evidence that the data are multifractal.

We then used the DTM Method to obtain the values of $\alpha = 1.6$, and $c1 = 0.06$ (Figure 26). Then from Eq. 10 we obtained a value of $H = 0.15$. As a check, we also fit the structure function (Eq. 6) directly (Figure 27), obtaining the values $\alpha = 1.7$, and $c1 = 0.04$ and $H = 0.1$. Differences between the parameter values obtained using the two approaches is too small to affect the multifractal simulations. Figure 27 directly reveals the multifractal nature of the Isleta data. For a monofractal (ordinary fractal), Eq. 6 become $\xi(q) = qH$; the structure function is linear. The concave downward curvature in Figure 27 clearly shows that the fractal parameters are changing with scale, hence the data are multifractal.

Finally, Figure 28 shows the data for our test portion of the Isleta data and compared with three realizations of the multifractal simulation using the fitted α, c1, and H parameter values. Recall that the goal is not to reproduce the exact noise pattern observed in the data, which is only one realization of a complex geologic process. The goal is to simulate geologic noise with the same statistical behavior as the data across all scales. Figure 28 shows that universal multifractal model captures this statistical behavior, minus the NS leveling errors and the remaining small UXO items. Furthermore, once the appropriate multifractal parameters have been obtained, we are in a position to simulate "Isleta-like" geologic noise on any desired scale, from centimeters to hundreds of kilometers.

Discussion and Conclusions

Summary of the Methodology and Case Histories

The basic premise of this work that we can improve UXO detection and discrimination by developing scale-independent models for the background noise created by soil and bedrock with large magnetic susceptibilities. Quality Assurance (QA) measures based on success rates at

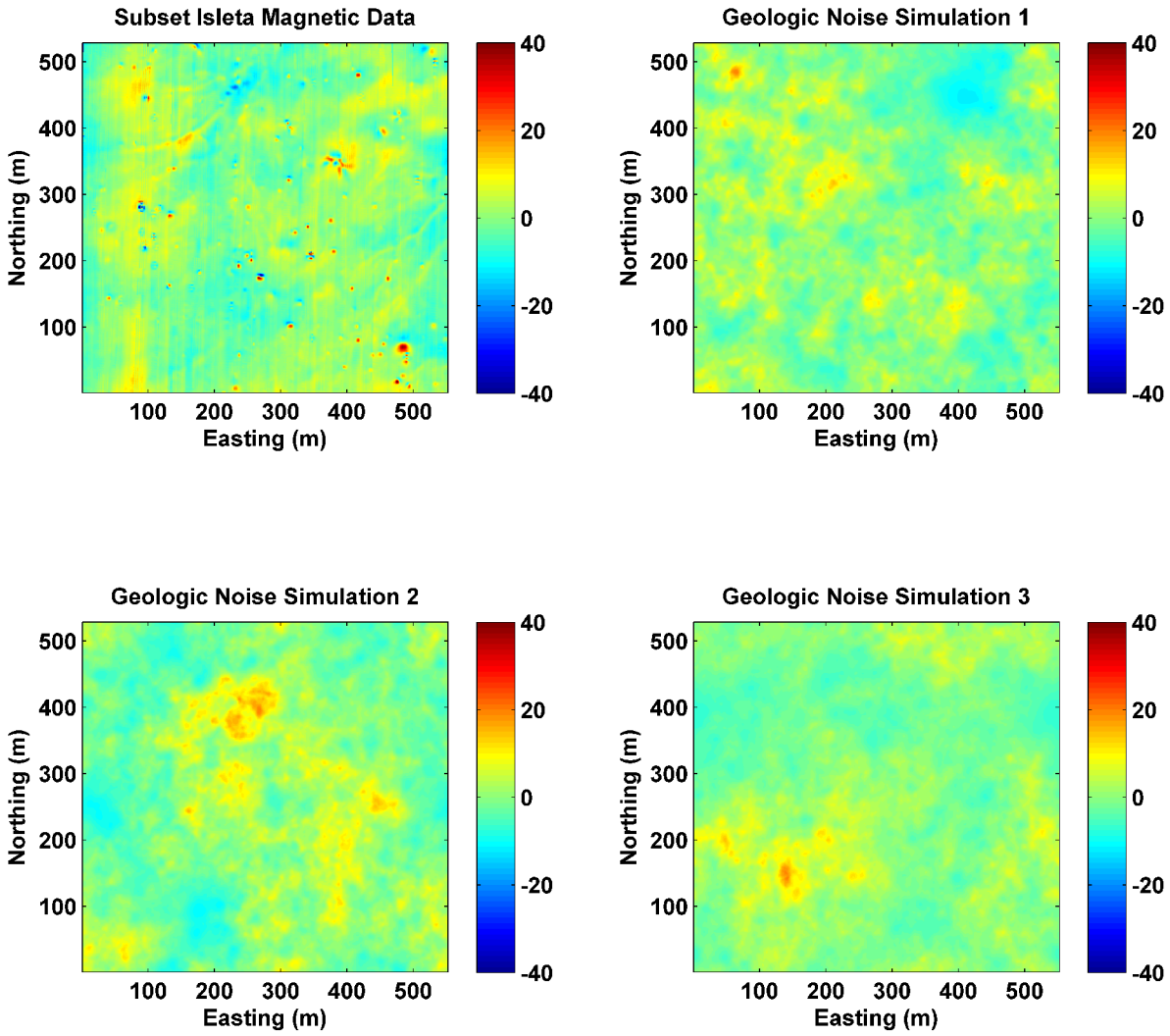

Figure 28: Isleta magnetic data (top left) and three multifractal realizations using the universal multifractal parameters fitted to the test data.

UXO proving grounds are unlikely to carry over to field studies because the local geology is different, and because geologic noise thresholds change with scale. This scaling problem is especially acute for wide-area surveys encompassing 10's or 100's of square kilometers, hence the need to develop mathematical models that can generalize measurements to larger or smaller scales.

Multifractal modeling is a well-established methodology for the representation of processes that scale across many orders of magnitude. In this pilot project we have demonstrated how to test whether the background magnetic susceptibilities are multifractal, how to then obtain the multifractal parameters α, c1, and H to fit a universal multifractal model, and how to use this model to generate simulations of the geologic background at any scale desired.

We applied the methodology to airborne magnetic data sets collected at three UXO sites with different levels of geologic magnetic noise: Sierra Army Depot, CA; Fort Ord, CA; and Pueblo of Isleta, NM. The geologic noise at Sierra Army Depot was extremely low, less than a nanoTesla, well below the magnetic noise level produced by the helicopter even after compensation. Improved UXO detection at such low-noise sites would require improved data acquisition before multifractal modeling would be useful.

Fort Ord magnetic data showed higher levels of magnetic noise, up to ± 20 nT or more. Our analysis showed that the data could be fit with a multifractal model, but that the magnetic background at this site is anisotropic. We produced reasonable anisotropic simulations with a fairly simple modification to our methodology. A more generalized approach would be required to incorporate, for example, a rotational anisotropy where the direction of anisotropy changes with scale. Generalized anisotropy is an issue we hope to address in future work.

The magnetic data collected at Pueblo of Isleta had the highest levels of geologic background noise of the three data sets we investigated, with levels reaching more than ± 40 nT for our test subset. Problems with magnetic background were noted by both the ORNL and NRL teams that flew surveys of this area. Again, the data proved to be multifractal, although in this case an isotropic simulation sufficed.

Limitations of this Pilot Study

One major challenge we faced in multifractal characterization of the airborne magnetic datasets collected at all three sites was determining the spectrum and multifractal parameters for the magnetic field produced by the geologic background in the presence of UXO-related magnetic anomalies. At each site we selected portions of the full data set with low concentrations of UXO, and in some cases fitted and removed UXO anomalies, but the possibility remains that the magnetic signatures of small UXO items were incorporated in our characterization of geologic noise. Ideally, we would like to see future investigations of UXO sites include collecting magnetic data over nearby regions with similar geology, but no history of ordnance activity. This would improve characterization of the geologic noise, but obviously would also increase the cost of data acquisition. However, the mobilization and demobilization costs would not change, so the incremental cost of collecting background data would be modest and, we believe, well worth the effort, particularly for sites with potentially high geologic noise where data quality assurance is especially import.

Secondly, because most contractors have focused their data processing stream on producing an optimal UXO anomaly map, the data we received were not processed for total magnetic field. Both ORNL (later this team moved to Battelle) and NRL used low-pass filtering to reduce instrument noise, helicopter noise, geologic background and other noise sources. Instead of producing total field maps, these researchers mapped residual magnetic field (e.g., Figure 14), analytic signal, or lists of anomaly targets. Because low pass filtering does not remove geologic anomalies with wavelengths comparable to the UXO, we think a better approach is to understand the full spectrum of the geologic noise, and for this we need the true total field data. As a consequence, we had to reprocess the raw data provided by the contractors to eliminate heading error, rotor noise, etc., to produce total field data. Unquestionably the contractors, who are more

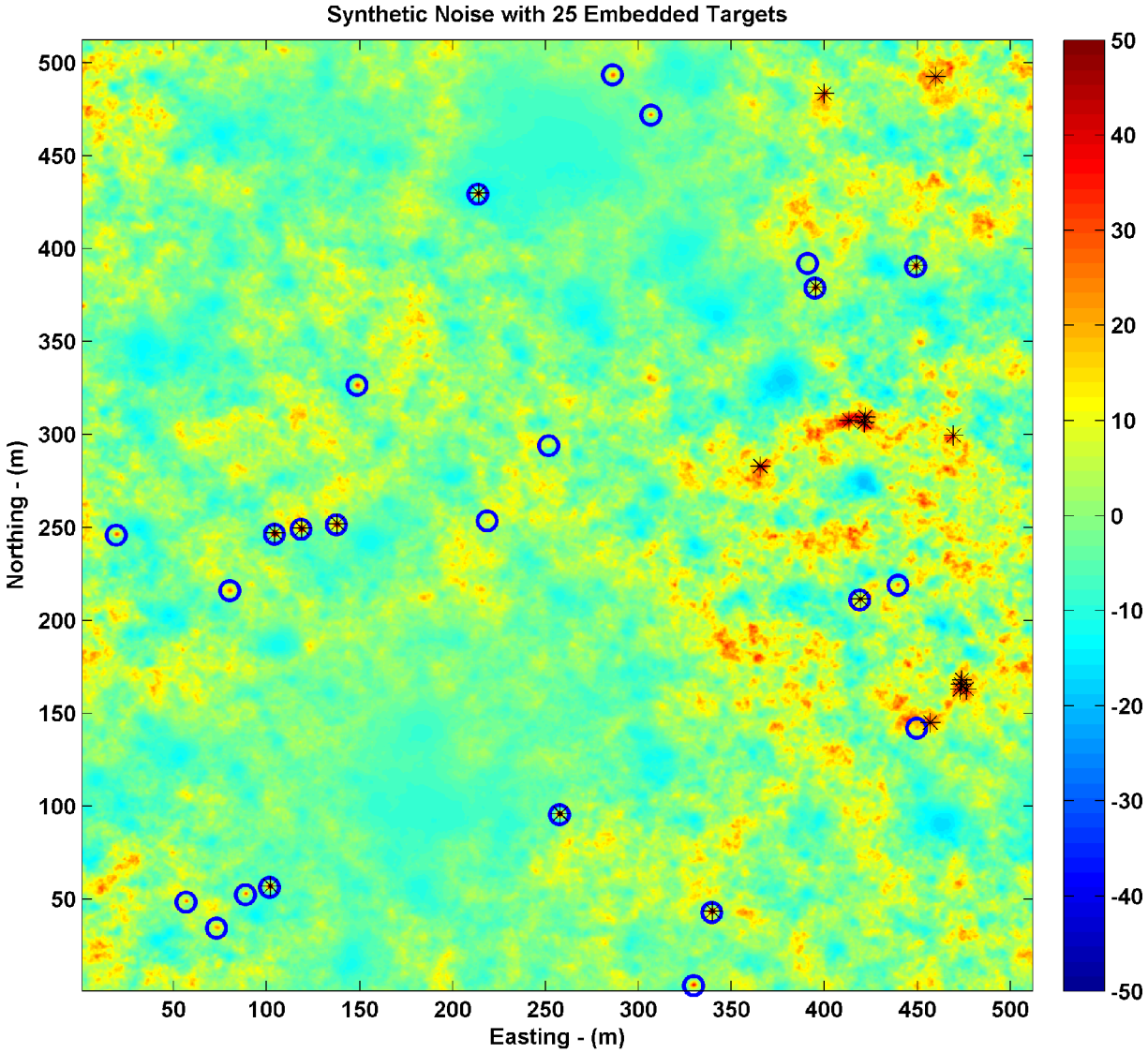

Figure 29: Simulated magnetic background (nanoTeslas) and dipole UXO targets. The actual locations of the targets are marked with blue circles. The anomalies identified by thresholding are marked with black asterisks. Numerous false positives and false negatives are evident.

cognizant of all the field data acquisition and processing steps, could have produced better total field data had they been tasked to do so as part of their original surveys.

A third limitation is the simplifying assumption that magnetic background could be approximated as coming entirely from thin surface layer, neglecting the distribution of magnetic susceptibilities as a function of depth. Pragmatically, this approximation can be justified because the magnetic field above the surface of the earth created by any 3-D distribution of magnetic susceptibilities can be treated as coming from an equivalent source layer at the surface (Blakely, 1996). Using a multifractal representation of an equivalent source layer in no way limits the simulations of the magnetic field. But because the equivalent source layer may bear little

resemblance to the true 3-D distribution of magnetic susceptibilities, it would be more rigorous to use a full 3-D multifractal representation of magnetic susceptibility, an endeavor that we wish to pursue.

Finally, as discussed, our current methodology assumes isotropy, or an anisotropy that can be modeled by simple stratification. The data set from Fort Ord demonstrated that isotropy is not always a valid assumption, and we were fortunate that in this case a simple representation of anisotropy produced simulations matching the character of the data at this site. However, developing an implementing a more general approach will be a priority in our future work.

Potential Applications

This pilot study focused on the developing methods for multifractal characterization and simulation of airborne magnetic data. The next steps include working on overcoming the limitations discussed above, and on application of the simulations to quality assurance (QA) for UXO detection and discrimination. To give an indication of how this work might progress, we created a simple example. Using the multifractal parameters we obtained for the S1 target area at Pueblo of Isleta, we simulated a 0.5 x 0.5 magnetic field at a flight height of 2.0 m, with 25 UXO targets embedded at random x-y locations, buried at depths of 0 to 1.5 m. The targets were approximated as simple dipoles with purely induced magnetic moments, and varied in strength from peak amplitudes of 8 – 150 nT. Consequently, some of the targets produced anomalies clearly above the magnetic background, others were buried in the noise. We then imported the this dataset into UXOlab and used thresholding at 35 nT to automatically locate anomalies. Figure 29 compares the actual target locations with the target picks. At this threshold, UXOlab pick 23 targets. Nine are correctly identified, 12 are false positives, and there are 14 false negatives. Clearly, statistics can be improved by manually eliminating picks clustering on the same peak, testing different thresholds, and using other peak picking algorithms. Furthermore, more sophisticated models of UXO items can be using in the forward simulation. The point, however, is that a realistic model for the geologic background facilitates “what-if” scenario testing and any scale, and the best choice of algorithms for a given site.

Future Work

The ability to create of realistic, site-specific data simulations allows the fine-tuning of detection and discrimination algorithms. The key next step is to develop collaborations with SERDP researchers working on these algorithms and customize our simulations to their needs. Some customizations would be straightforward, such as simulating measurements collected along irregular flight paths and at uneven altitudes, or simulating vertical magnetic gradient data. Others enhancements would require further research.

We have already discussed the need to incorporate a generalized anisotropy in the multifractal simulations. To do this also requires improved data characterization, going beyond the double trace moment method and isotropic fitting of the structure function. A number of approaches to extracting anisotropic multifractal parameters have been discussed in the literature (e.g., Lewis, et al., 1999; Tennekoon et al., 2003; Cheng, 2004), and these need to be investigated for this application.

UBC researchers have found that one of the more reliable methods of distinguishing between natural and UXO-related anomalies is to examine the orientation of the anomaly's dipole field (e.g., Billings, 2004). UXO are more likely to have dipole moment oriented differently than the inducing field. To test this we would need to refine our magnetic model to allow for the inclusion of remnant magnetism in the simulated geologic background.

Finally, we would like to point out that the multifractal simulation approach we have applied in this pilot study is not limited to the simulation of magnetic susceptibility. It is feasible to develop simulations for physical properties that govern other commonly used UXO detection methods such as electrical conductivity (electromagnetic methods) or dielectric properties (ground penetrating radar). The study of correlated multifractal fields is a relatively new research area. Marsan et al. (1996) discussed the theory for correlated multifractal fields, but we are not aware of any work that addressed the problem in an applied sense. Development of joint multifractal simulation of multiple, linked geophysical quantities would facilitate the current trend toward data fusion approaches to UXO detection and discrimination.

Acknowledgments

We would like to thank Bill Doll and Jeff Gamey (Battelle) for providing helicopter magnetic data all three case study sites and sharing their data processing expertise. Herb Nelson (NRL), Daniel Steinhurst (NRL contractor) provided MTADS airborne data for the Isleta site, and processing guidance. Doug Oldenburg (UBC) graciously granted a free license to use UXOlab for this project, and David Sinex (UBC) provided training and support. We also benefited from useful discussions with Yaoguo Li (Colorado School of Mines) on the subject of magnetic background noise. Temple graduate students Durgesh Sinha and Jiabin Xue worked hard on Matlab code development efforts and computer simulations. Finally, we would like to thank the SERDP program office for their continued support throughout this project.

References

Baveye P., C.W. Boast, S. Ogawa, J-Y. Parlange, and T. Steenhuis. 1998. Influence of image resolution and thresholding on the apparent mass fractal characteristics of preferential flow patterns in field soils. *Water Resources Research* **34**:2783–2796.

Billings, S.D. 2004. Discrimination and classification of buried unexploded ordnance using magnetometry, *IEEE Trans. Geosci. Remote. Sen.* **42,6**:1241-1251.

Billings, S.D., L.R. Passion, and D.W. Oldenburg. 2002. Discrimination and identification of UXO by geophysical inversion. Phase II: Inversion of total-field magnetics. Final Progress Report, pp. 48.

Blakely, R. J. 1996. Potential theory in gravity & magnetic applications. Cambridge University Press, Cambridge, United Kingdom, pp. 441.

Boufadel, M. C., S. Lu, F. J. Molz and D. Lavallée. 2000. Multifractal scaling of the intrinsic permeability, *Water Resources Res.*, **36:**3211-3222.

Butler, D. 2001. Potential field methods for location of unexploded ordnance. *The Leading Edge*, **20** (8): 890-895.

Butler, D. 2003. Implications of magnetic background for unexploded ordnance detection. *Journal of Applied Geophysics*, **54**: 111-125.

California. 2003. California's Groundwater, Bulletin 118 (2003 Update). California Department of Water Resources, 245pp.

Cheng, Q. M. 2004. A new model for quantifying anisotropic scale invariance and for decomposition of mixing patterns. Mathematical Geology 36, (3) (APR): 345-60.

Davis A., A. Marshak, W. Wiscombe, R. Cahalan. 1994. Multifractal characterizations of nonstationarity and intermittency in geophysical fields: Observed, retrieved, or simulated. *J Geophys. Res.* **99**: 8055–8072.

Davis A., A. Marshak, W. Wiscombe, and R. Cahalan. 1996. Scale invariance of liquid water distributions in marine stratocumulus, part I, Spectral properties and stationary issues. *J Atmos. Sci.* **53**:1538–1558.

Davis, K., Y. Li, and M. Nabighian. 2005. Automatic detection of UXO anomalies using Euler deconvolution. Society of Exploration Geophysics Technical Abstracts, 1133-1136.

Frisch, U., and G. Parisi. 1985. On the singularity structure of fully developed turbulence. In: Ghil M, Benzi R, Parisi G (eds) Turbulence and predictability in geophysical fluid dynamics.

Elsevier, New York, pp 84–88.

Grigoriu, M. 1995. Applied non-gaussian processes: examples, theory, simulation, linear random vibration, and MATLAB solutions. Prentice-Hall, Englewood Cliffs, 442 pp.

Gupta V.K., and E. Waymire. 1990. Multiscaling properties of spatial rainfall and river flow distribution. *J. of Geophys. Res.* **95**(D3):1999–2009.

Hewett T.A.1986. Fractal distribution of reservoir heterogeneity and their influence on fluid transport. *in*: 61st annual technical conference, Soc. of Pet. Eng., Richardson.

Kolmogorov, A.N. 1962. A refinement of previous hypotheses concerning the local structure of turbulence in a viscous incompressible fluid at high Reynolds number. J Fluid Mech **13**:82–85.

Lavallée D. 1991. Multifractal analysis and simulation technique and turbulent fields. PhD Thesis. Dep. of Physics, McGill University, 133 pp.

Lavallée D., S. Lovejoy, D. Schertzer, and P. Ladoy. 1993. Nonlinear variability and landscape topography: analysis and simulation. *In*: De Cola L, Lam N (eds) Fractals in Geography. Prentice-Hall, Englewood Cliffs, pp. 158–192.

Lewis, G. M., S. Lovejoy, D. Schertzer, and S. Pecknold. 1999. The scale invariant generator technique for quantifying anisotropic scale invariance. *Computers & Geosciences* 25, (9; 9) (11): 963.

Li, Y., R. Krahenbuhl, and T. Meglich. 2006. Improving UXO detection and discrimination in magnetic environments. Annual Progress Report, SERDP MM-1414, pp. 64.

Liu H.H., Molz F.J. 1997. Multifractal analyses of hydraulic conductivity distributions. *Water Resources Res.* **33**:2483–2488.

Lovejoy S., D. Lavallée, D. Schertzer D, and P. Ladoy. 1995. The $l^{1/2}$ law and multifractal topography: Theory and analysis. *Nonlinear Processes Geophys* **2**:16–22.

Lovejoy, S., S. Pecknold, and D. Schertzer. 2001. Stratified multifractal magnetization and surface geomagnetic fields – I. Spectral analysis and modelling. *Geophys J. Int.*, **145:**112-126.

B. Mandelbrot. 1967. How Long Is the Coast of Britain? Statistical Self-Similarity and Fractional Dimension. *Science*, New Series, **156**(3775): 636-638.

Maus, S., K.P. Sengpiel, B. Rottger, B. Siemon and E.A.W. Tordiffe. 1999. Variogram analysis of helicopter magnetic data to identify paleochannels of the Omaruru river, Namibia. *Geophysics*, **64**: 785-794.

Marsan, D. and C. Bean. 2003. Multifractal modeling and analyses of crustal heterogeneity, In: Heterogeneity in the Crust and Upper Mantle: Nature, Scaling and Seismic Properties, Goff, J.A. and K. Holliger (eds), Kluwer Academic Publishers, pp. 349.

Marsan D., Schertzer, D., and Lovejoy, S., 1996, Causal space-time multifractal process: predictability and forecasting of rain fields, *J. Geophys. Res.* **101**(D21):26333-26346.

Meneveau C., and K.R. Sreenivasan. 1987. The multifractal spectrum of the dissipation field in turbulent flows. Nucl Phys B Proc Suppl **2**:49–76.

Monin, A.S., and A.M. Yaglom. 1975. Statistical fluid mechanics: mechanics of turbulence. The MIT Press, 900 pp.

Molz F.J., and Boman G. 1993. A fractal-based stochastic interpolation scheme in subsurface hydrology. *Water Resources Res.* **29**:3769–3774.

Molz F.J., and Boman G. 1995. Further evidence of fractal structure in hydraulic conductivity distributions. *Geophys. Res. Lett.* **22**:2545–2548.

Nelson, H.H. 2003. MTADS airborne and vehicular survey of target S1 at Isleta Pueblo, Albuquerque NM, 17 February-1 March 2003, Naval Research Laboratory, NRL/MR/6110—04-8764, pp. 46.

Neuman S.P. 1990. Universal scaling of hydraulic conductivities and dispersivities in geologic media. *Water Resources Research*, **26**(8):1749–1758.

Nikias, C.L., and M. Shao. 1995. Signal processing with alpha-stable distributions and applications. Wiley, New York, 184 pp.

Obukhov A. 1962. Some specific features of atmospheric turbulence. *J Geophys Res* **67**:3011–3014.

ORNL. 2003. Airborne geophysical survey for unexploded ordnance at Sierra Army Depot, California, Draft Final Report, Prepared by the Environmental Sciences Division, Oak Ridge National Laboratory, for USACE, Huntsville, pp. 19.

ORNL. 2004. Final report on 2003 airborne geophysical survey at Pueblo of Isleta bombing targets, New Mexico. Prepared by the Environmental Sciences Division, Oak Ridge National Laboratory, ESTCP Projects 200037 and 37, pp. 48.

Painter S., and L. Paterson. 1994. Fractional Levy motion as a model for spatial variability in sedimentary rocks. *Geophys. Res. Lett.* **21**:2857–2860.

Pecknold S., S. Lovejoy, D. Schertzer, C. Hooge, and J.F. Malouin. 1993. The simulation of

universal mulfractals. In: Cellular Automata: Prospects in Astronomy and Astrophysics, J.M. Perdang and A. Lejeune (eds), World Scientific, 228-267.

Pecknold, S., S. Lovejoy, and D. Schertzer. 2001. Stratified multifractal magnetization and surface geomagnetic fields – II. Multifractal analysis and simulation. *Geophys. J. Int.* **145**:127-144.

Perrier E., M. Rieu, G. Sposito, G. de Marsily. 1996. Models of the water retention curve for soils with a fractal pore size distribution. *Water Resources Research* **32**:3025–3031.

Phillips, O.M. 1985. Spectral and statistical properties of the equilibrium range in wind-generated gravity waves. J Fluid Mech **156**:505–531

Pilkington, M. and J.P. Todoeschuck. 1993. Fractal magnetization of continental crust, *Geophys. Res. Lett.*, **20**: 627-630.

Pilkington, M. and J.P. Todoeschuck. 1995. Scaling nature of crustal susceptibilities, *Geophys. Res. Lett.*, **22**, 779-782.

Putnam, J. 2001. Kaho'olawe program management and technology. In *Proc. UXO Forum*, 2001.

Sanchez, V., Y. Li, M. Nabighian, and D. Wright. 2006. Relative importance of magnetic moments in UXO clearance applications. Society of Exploration Geophysics Technical Abstracts: 1381-1385.

Schertzer D., Lovejoy S. 1987. Physical modeling and analysis of rain and clouds by anisotropic scaling multiplicative processes. *J Geophys Res* **92**:9693–9714.

Schmitt F., S. Lovejoy, and D. Schertzer. 1995. Multifractal analysis of the Greenland ice-core project climate data. *Geophys. Res. Lett.* **22**(13):1689–1692.

Tennekoon, L., M.C. Boufadel, D. Lavallée and J. Weaver. 2003. Multifractal anisotropic scaling of the hydraulic conductivity, *Water Resources Res.*, **39**: 1193-1205.

Tennekoon, L., M.C. Boufadel, and J. E. Nyquist. 2004. Results of preliminary investigations into multifractal analysis of airborne geophysical data. *Proc. SEG Int'l Exposition and 74th Annual Meeting,* Denver, Colorado, pp. 4.

Tennekoon, L., M.C. Boufadel, and J. E. Nyquist. 2005. Multfractal characterization of airborne geophysical data at the Oak Ridge facility. *Stoch. Environ. Res. Risk Assess,* **19**: 227-239.

Tchiguirinskaia, I., S. Liu, F.J. Molz, T.M. Williams, and D. Lavallée. 2000. Multifractal versus monofractal analysis of wetland topography. Stochastic Env. Res. and Risk Assessment, 14:8-32.

UBC-GIF uxo software. [cited 2/25/2008 2008]. Available from http://www.eos.ubc.ca/ubcgif/uxo/software.html (accessed 2/25/2008).

Uchaikin, V.V., Zolotorev V.M. 1999. Chance and stability, stable distributions and their applications. VSP, Utrecht, Netherlands, 596 pp.

Van, G.P., G. Calvert, L.P. Beard, T.J. Gamey, and A. M. Emond, 2004, Validation of Helicopter-Based Magnetic Survey at the Former Badlands Bombing Range: Expanded abstract in Proceedings of the Sixth Monterey Demining Symposium (MINWARA): Monterey, California, May 09-13, 2004.

Wilson, J., D. Schertzer, and S. Lovejoy. 1991. Physically based cloud modeling by multiplicative cascade processes. *In Non-Linear Variability in Geophysics: Scaling and Fractals*, D. Schertzer and S. Lovejoy, eds. Dordrecht, The Netherlands: Kluwer.

Xu, S., Yang, J., Yang, C., Xiao, P., Chen, S., and Guo, Z. 2007. The iteration method for downward continuation of a potential field from a horizontal plan. *Geophys. Prospecting*, **55**: 883-889.

Yaglom, A.M. 1987. Correlation theory of stationary and related random functions I: Basic Results. Springer-Verlag, Berlin, Heidelberg, and New York, 526 pp.